IEEE Access
Multidisciplinary | Rapid Review | Open Access Journal

Received March 20, 2019, accepted April 16, 2019, date of publication April 23, 2019, date of current version May 3, 2019.

Digital Object Identifier 10.1109/ACCESS.2019.2912905

Representation Space Analytical Method for Path Planning of Free-Floating Space Manipulators

QINGXUAN JIA, (Member, IEEE), BONAN YUAN, AND GANG CHEN, (Member, IEEE)
School of Automation, Beijing University of Posts and Telecommunications, Beijing 100876, China

Corresponding author: Gang Chen (buptcg@163.com)

This work was supported by the National Natural Science Foundation of China under Grant 61403038, Grant 61573066, and Grant 61327806.

ABSTRACT Path planning is necessary for free-floating space manipulators to perform space tasks. However, the coupled motion between manipulator and base directly acts on path planning procedure, which results in current manipulator motion state is dependent on previous motion state, so we must consider the control of base-coupled motion in path planning. In this paper, we propose a general path planning strategy for free-floating space manipulators based on the representation space (RS) analytical method. RS consists of the representation variables which are connected to task attributes and base-coupled motion simultaneously, and it can be utilized to check task realizability and construct a path planning domain for free-floating space manipulators. To analyze the effects of base-coupled motion on path planning, we classify RS into five types according to different base control modes: fixed vehicle RS (FRS), attitude constrained RS (CRS), maximum reachable RS (MRS), guaranteed RS (GRS), and partly guaranteed RS (PGRS). CRS tells us the variation of base attitude (instead of base centroid position) directly influences task realizability and path planning, so we should particularly consider the control of motion of base attitude in path planning. With appropriately considering the control of base attitude and satisfying the base attitude deflection limitation, only PGRS can be utilized to check task realizability and construct a path planning domain for free-floating space manipulators. Then, we design a path planning strategy in PGRS based on A* algorithm. Finally, we apply the RS analytical method to the 3-DOF free-floating space manipulator to visually show RS, and the effectiveness of the method is verified by a simulation experiment. The RS analytical method is appropriate to path planning for any kinds of manipulators and various tasks. We only need to select the suitable representation variables, which can faithfully reflect task and manipulator attributes.

INDEX TERMS Space manipulators, path planning, representation space, representation variables, task realizability evaluation.

I. INTRODUCTION

With strong flexibility and outstanding working performance, space manipulators are widely used in various space tasks [1]–[4]. Generally speaking, space manipulators are installed on spacecrafts which are called ''Base''. There are several base control modes, including ''Fixed Base'' (base is fully fixed, and its position/attitude are constant), ''Attitude Constrained Base'' (base attitude is constant, but its position is variable), and ''Free-floating Base'' (base floats freely in space, and the motions between base and manipulator are coupled) [5]. ''Fixed Base'' and ''Attitude Constrained Base'' modes require the spacecraft to apply extra force/moment to limit base-coupled motion, so these two base control modes will consume many precious resources. To save resources, base is usually free-floating.

In order to make space manipulators finish task successfully, path planning, which is to find an executable path from an initial state to a desired state under some predefined requirements and constraints in a specific planning domain, is necessary [6]–[8]. However, if the assigned task is implicitly unrealizable, path planning is meaningless. Therefore, it's necessary to check task realizability before path planning. If the task is realizable, we construct a reasonable path planning domain through deleting the manipulator system states that don't meet the predefined requirements

The associate editor coordinating the review of this manuscript and approving it for publication was Yangming Li.

and constraints. Then an executable path can be searched in this domain.

Traditional path planning is generally conducted in joint space [9], [10] and Cartesian space [11], [12]. Surrounding these two kinds of space, many indexes are established to depict working performance of manipulator system states. Task realizability can be checked by comparing the working performance with predefined task requirements and constraints. By deleting the manipulator system states whose working performance doesn't meet the requirements, a path planning domain is constructed. To be specific, in joint space, the minimum singular value, manipulability and condition number based on the Jacobian matrix were proposed to depict the dexterity of manipulators [13], [14]. For free-floating space manipulators, the indexes above were derived from the generalized Jacobian matrix [15]. By deleting the configurations closing to singularity, a path planning domain in joint space was constructed [16]. In Cartesian space, workspace was utilized to assess positional reachability of end-effector [17], [18]. For free-floating space manipulators, Umetani and Yoshida [15] and Vafa and Dubowsky [19] classified workspace into 4 types according to different base control modes. By deleting unreachable points in workspace, a path planning domain in Cartesian space was constructed.

The researches above only gave some individual indexes to depict working performance in a single aspect, but space tasks usually had simultaneous requirements for working performance of space manipulators in multiple aspects. Aiming at specific space tasks, Chen *et al.* [20], [21] and Jia *et al.* [22] established a comprehensive kinematics performance index through integrating multiple individual indexes together to evaluate task realizability and construct a path planning domain for fixed-base space manipulators. For example, for end-effector transferring tasks, they integrated the mini-mum singular value, condition number and manipulability into workspace to comprehensively depict dexterity in workspace of manipulators. Deleting the end-effector point with poor dexterity, they construct a path planning domain. Then the reachable path of end-effector with the best dexterity was obtained. Their researches only focused on fixed-base space manipulators performing one type task. But space tasks had varying requirements and constraints, so the comprehensive kinematics performance index should always be rebuilt for different tasks. Therefore, researches above were not general to various space tasks.

To find a general task realizability evaluation and path planning domain construction method, some researches established state space for path planning of robots. This method specifically selects the system variables which were connected to task attributes as state variables. By deleting the state variables which didn't meet task requirements and constraints, the state space for path planning is constructed. State space was widely utilized in searching an obstacle-free path for mobile robots [23], [24]. Zhang *et al.* [25] dynamically adjusted the dimensionality of state space according to environment changes, and obtained the continuous and smooth path in a large outdoor environment for a mobile robot. Xie *et al.* [26] integrated the relative position relations among multiple mobile robots into state space, and created a collection of the coordinated motion paths for the multi-robot system. In recent years, some scholars have tried to utilize state space for path planning of manipulators. Selecting state variables for a 2-DOF fixed-base manipulator, and deleting those colliding with obstacles, Xie [27] established the reachable state space, and obtained an obstacle-avoidance path through A* algorithm. Yovchev *et al.* [28] took all dynamic characteristics of manipulator into consideration to establish state space, and constructed a path planning domain by iterative learning method. Task realizability evaluation and path planning domain construction based on state space are independent of specific task requirements and constraints, so path planning in state space is comprehensive for various tasks. However, the method doesn't consider the internal dependency among the selected state variables. Sometimes state space even consists of some relative state variables, so its dimensionality is always very high, and path planning in state space is accompanied by huge computational burden.

In fact, the dependency among state variables does exist, which means the state variables can be simplified. To reduce redundant state variables, Su and Xie [29] put forward the Representation Space (RS) analytical method for path planning. He selected the fewest independent system variables which could accurately reflect task attributes as Representation Variables to construct RS. By deleting the representation variables that didn't meet the predefined task requirements and constraints, a path planning domain was obtained. The reachable region in RS reflected the ability of manipulator to accomplish tasks. And task execution can be regarded as the transition of system state from the initial representation to the goal in RS. Hence, path planning is rendered as a trajectory searching problem in RS. Selecting end-effector positon/attitude as representation variables, Su constructed RS of a 2-DOF fixed-base manipulator, and conducted task realizability evaluation and path planning in RS. Following Su's research, Wu and Su [30] selected joints angle as representation variables to construct RS, and analyzed the influences of obstacles distribution on task realizability. The RS analytical method also gave a universal task realizability evaluation and path planning domain construction method, and it had less computational complexity than that of state space. However, the existing researches only aimed at fixed-base manipulators. For free-floating space manipulators, the motions between base and manipulator are intensely coupled, so the space manipulator system possesses nonholonomic behavior [31], [32]. When space manipulators perform tasks, base will be disturbed. Large base disturbance will influences communication quality between the spacecraft and mission control, and even threaten spacecraft stability. Therefore, to avoid large base disturbance, the RS analytical method must consider the control of base-coupled motion.

In this paper, we propose the RS analytical method to check task realizability and construct a path planning domain

for free-floating space manipulators. We utilize the Virtual Manipulator (VM) method to establish kinematics model of space manipulators at first. Then we select the system variables which are connected to task requirements and base-coupled motion as representation variables to construct RS. Now that the base-coupled motion influences task realizability and acts on path planning, we may construct different types of RS by changing the base-coupled motion characteristic. Then, according to the attributes of different types of RS, the effects of base-coupled motion on RS construction and path planning can be known. Referring to classifying workspace of space manipulators based on different base control modes in [15] and [19], we construct 5 types of RS according to different base control modes. Task realizability evaluation and path planning domain construction can be performed in a certain type of RS, and path planning is accomplished by A* algorithm [33]. For high-DOF space manipulators, the dimensionality of RS is too high to be drawn, so we apply the RS analytical method to the 3-DOF free-floating space manipulator. Aiming at the end-effector transferring task, we select end-effector position/attitude as representation variables to visually show RS.

5 types of RS include Fixed Vehicle RS (FRS), Attitude Constrained RS (CRS), Maximum Reachable RS (MRS), Guaranteed RS (GRS) and Partly Guaranteed RS (PGRS). Different types of RS have different effects on task realizability evaluation and path planning:

FRS is for fixed-base manipulators. It can only be used to check the task realizability and construct a path planning domain for the space manipulator whose base position/attitude are fixed. CRS is for space manipulators whose base attitude is fixed, so it can't be applicable to free-floating space manipulators. But it illustrates that the variation of base attitude influences task realizability and path planning of free-floating space manipulators, so we should control the coupled motion of base attitude in path planning for free-floating space manipulators. MRS is constructed with all theoretically reachable representation variables of free-floating space manipulators, but it entirely neglects the control of base-coupled motion, so we can't evaluate task realizability and plan path in MRS. GRS consists of the representation variables where space manipulators reach with base attitude taking any values in theoretical range $\Psi_{0x} \in [-180°, 180°]$, $\Psi_{0y} \in [-180°, 180°]$, $\Psi_{0z} \in [-180°, 180°]$ (where Ψ_{0x}, Ψ_{0y}, Ψ_{0z} are base attitudes in x, y, z axis). However, GRS excessively considers the control of base-coupled motion, so it is small or even empty. Path planning is prone to fail in GRS. But in the practical application, base attitude deflection must be limited in a certain range. To satisfy the practical base attitude deflection limitation, we calculate the practical reachable range of base attitude. Finding out the representation variables where manipulators can reach with base attitude taking any value in the practical reachable range, we construct PGRS. Because appropriately considering the practical limitation of base attitude deflection, PGRS is suitable for checking task realizability and serving as a path planning domain for free-floating space manipulators. When space manipulators track the path in PGRS, we need to limit base attitude in the practical reachable range through the non-holonomic motion planning method.

The research in this paper possesses the following traits:

1 The RS analytical method for task realizability evaluation and path planning domain construction of free-floating space manipulators is proposed for the first time.

2 According to different base control modes, we construct 5 types of RS. And PGRS can be applied to task realizability and construct a path planning domain. The executable path for free-floating space manipulator is finally found in PGRS.

3 Because representation variables are artificially selected according to task attributes and manipulator characteristics, the RS analytical method is universal to various tasks and manipulators, despite of DOFs or installed on base with any control modes. For the specific task and manipulator, we only need to select the reasonable representation variables to establish RS.

The remaining of this paper is organized as follows: In Section II, we establish the equivalent VM of free-floating space manipulators. Then definition of RS for free-floating space manipulators is given, and 5 types of RS are constructed. Then the effects of different types of RS on task realizability and path planning domain construction of space manipulators is analyzed. The path planning strategy based on A* algorithm is designed in Section III. To help readers understand the RS analytical method, we task the 3-DOF free-floating space manipulator as an example, and select end-effector position/attitude as representation variables to show RS in Section IV. Simulation experiment is designed to verify the effectiveness and practicability of the RS analytical method. The conclusion is in Section V.

II. REPRESENTATION SPACE OF FREE-FLOATING SPACE MANIPULATORS

RS analytical method is universal for task realizability evaluation and path planning domain construction of manipulators. It selects the fewest independent manipulator system variables which are connected to task attributes as representation variables to construct RS. For free-floating space manipulators, the base-coupled motion will directly influence path planning, so we should select the representation variables which can are connected to the base-coupled motion and task attributes simultaneously. Sometimes the base-coupled motion is directly selected as representation variables.

In this section, we establish the VM which is kinematically equivalent to free-floating space manipulators at first. Then we introduce the traditional RS analytical method of fixed-base manipulators. Considering the control of base-coupled motion, we define RS for free-floating space manipulators. According to different base control modes, we classify RS of the space manipulators into 5 types. Finally, the effects of different types of RS on task realizability evaluation and path planning of free-floating space manipulators are analyzed in detail.

A. THE EQUIVALENT VM OF FREE-FLOATING SPACE MANIPULATORS

We give the equivalent VM of the n-DOF(degree of freedom) free-floating space manipulator in this section. Readers can find the detailed kinematics modeling process in Appendix.

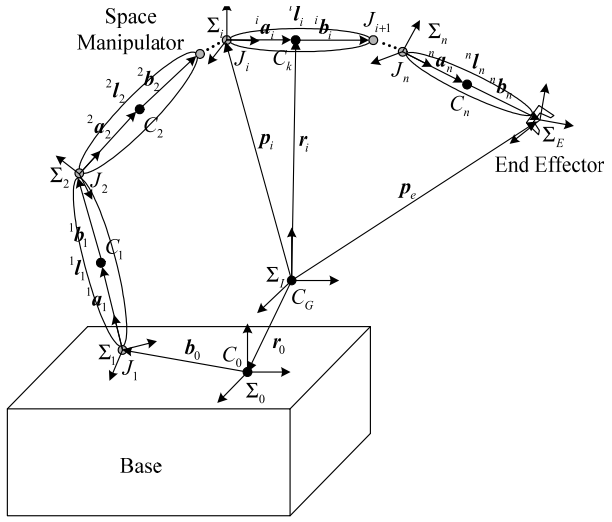

FIGURE 1. Kinematics model of the *n* -DOF free-floating space manipulator.

The n-DOF free-floating space manipulator is shown in Fig.1. All joints are rotational. The vectors and matrixes with subscript in the upper left corner are with respect to corresponding coordinates, and the others with no subscript in the upper left corner are with respect to inertial coordinate.

Where

C_0	base centroid
C_i	centroid of the i-th link
C_G	centroid of the space manipulator system
J_i	i-th joint
$\sum_I$	inertial coordinate frame built inC_G
$\sum_0$	coordinate frame built in base centroid
$\sum_i$	coordinate frame built in the i-th joint, $i = 1, 2, \cdots, n$
$\sum_E$	end-effector coordinate frame
$\boldsymbol{p}_i \in \mathbf{R}^{3\times1}$	position of J_i, $i = 1, 2, \cdots, n$
$\boldsymbol{p}_e = [x_e, y_e, z_e]^{\mathrm{T}} \in \mathbf{R}^{3\times1}$	position of end-effector
$\boldsymbol{\Psi}_e = [\alpha_e, \beta_e, \gamma_e]^{\mathrm{T}} \in \mathbf{R}^{3\times1}$	attitude of end-effector
$\boldsymbol{r}_i \in \mathbf{R}^{3\times1}$	position of C_i, $i = 1, 2, \cdots, n$
$\boldsymbol{r}_g \in \mathbf{R}^{3\times1}$	position of C_G, $\boldsymbol{r}_g = \sum_{i=0}^{n} m_i \boldsymbol{r}_i \Big/ M$. We build $\sum_I$ in C_G, so when momentum is conservative, $\boldsymbol{r}_g \equiv \mathbf{0}$
$\boldsymbol{r}_0 \in \mathbf{R}^{3\times1}$	position of C_0
$\boldsymbol{\Psi}_0 \in \mathbf{R}^{3\times1}$	base attitude
$\boldsymbol{b}_0 \in \mathbf{R}^{3\times1}$	position vector from C_0 to J_1
${}^i\boldsymbol{a}_i \in \mathbf{R}^{3\times1}$	position vector from J_i to C_i, $i = 1, 2, \cdots, n$
$\boldsymbol{a}_i \in \mathbf{R}^{3\times1} \boldsymbol{a}_i = \boldsymbol{r}_i(\boldsymbol{\Psi}_0, \theta_1, \cdots, \theta_i){}^i\boldsymbol{a}_i, a_i$	is its module, $i = 1, 2, \cdots, n$
${}^i\boldsymbol{b}_i \in \mathbf{R}^{3\times1}$	vector from C_i to J_{i+1}, $i = 1, 2, \cdots, n$
$\boldsymbol{b}_i \in \mathbf{R}^{3\times1} \boldsymbol{b}_i = \boldsymbol{r}_i(\boldsymbol{\Psi}_0, \theta_1, \cdots, \theta_i){}^i\boldsymbol{b}_i, b_i$	is its module, $i = 1, 2, \cdots, n$
${}^i\boldsymbol{l}_i \in \mathbf{R}^{3\times1}$	vector from J_i to J_{i+1}, $i = 1, 2, \cdots, n$
$\boldsymbol{l}_i \in \mathbf{R}^{3\times1} \boldsymbol{l}_i = \boldsymbol{a}_i + \boldsymbol{b}_i, l_i$	is its module, $i = 1, 2, \cdots, n$

For free-floating space manipulators, its momentum is always conservative, and the linear momentum is integrable, so the end-effector position/attitude $[\boldsymbol{p}_e, \boldsymbol{\Psi}_e]$ are only related to manipulator configuration $\boldsymbol{\theta}$ and base attitude $\boldsymbol{\Psi}_0$, instead of position of base centroid $\boldsymbol{r}_0$, i.e. $[\boldsymbol{p}_e, \boldsymbol{\Psi}_e]^{\mathrm{T}} = [\boldsymbol{p}_e(\boldsymbol{\Psi}_0, \boldsymbol{\theta}), \boldsymbol{\Psi}_e(\boldsymbol{\Psi}_0, \boldsymbol{\theta})]^{\mathrm{T}}$. End-effector position is expressed as

$$\boldsymbol{p}_e = \frac{m_0}{M}\boldsymbol{b}_0 + \left(\frac{m_0}{M}\boldsymbol{a}_1 + \frac{m_0+m_1}{M}\boldsymbol{b}_1\right) + \cdots + \left(\left(\sum_{i=1}^{n-1} m_i \Big/ M\right)\boldsymbol{a}_n + \boldsymbol{b}_n\right) \quad (1)$$

where m_0 is base mass, m_i is mass of the i-th link, and M is the total mass of overall system, i.e. $M = \sum_{i=0}^{n} m_i$.

Making

$$\hat{\boldsymbol{a}}_i = \frac{\sum_{q=0}^{i-1} m_q}{M}\boldsymbol{a}_i, \quad i = 1, 2, 3, \cdots, n$$

$$\hat{\boldsymbol{b}}_j = \frac{\sum_{q=0}^{j} m_q}{M}\boldsymbol{b}_j, \quad j = 0, 1, 2, 3, \cdots, n$$

$$\hat{\boldsymbol{l}}_k = \hat{\boldsymbol{a}}_k + \hat{\boldsymbol{b}}_k, \quad k = 1, 2, 3, \cdots, n$$

Thus $\boldsymbol{p}_e = \hat{\boldsymbol{b}}_0 + \sum_{i=1}^{n}(\hat{\boldsymbol{a}}_i + \hat{\boldsymbol{b}}_i)$. $\hat{\boldsymbol{a}}_i$, $\hat{\boldsymbol{b}}_j$ and $\hat{\boldsymbol{l}}_k$ are links parameters of the VM, and they are in the same directions with $\boldsymbol{a}_i$, $\boldsymbol{b}_j$ and $\boldsymbol{l}_k$. VM is installed on the virtual ground by a passive spherical joint which represents the coupled motion of base attitude. Fig.2 shows the equivalent VM.

B. DEFINITION OF RS FOR FREE-FLOATING SPACE MANIPULATORS

We introduce RS for fixed-base manipulators at first. RS is a higher-dimensional space created by the representation variables which can accurately reflect the task attributes. Assuming $\xi_1, \xi_2, \cdots, \xi_m$ are the selected representation variables, and they meet $\xi_i^{\min} \le \xi_i \le \xi_i^{\max} (i = 1, 2, \cdots, m)$, where $\xi_i^{\min}$ and $\xi_i^{\max}$ are lower and upper limits of the i-th representation variable. Representation variables form a vector $\boldsymbol{\xi} = [\xi_1, \xi_2, \cdots, \xi_m]^{\mathrm{T}} \in \mathbf{R}^m$, and we call $\boldsymbol{\xi}$ the generalized coordinate of representation variables (GCRV). RS is the

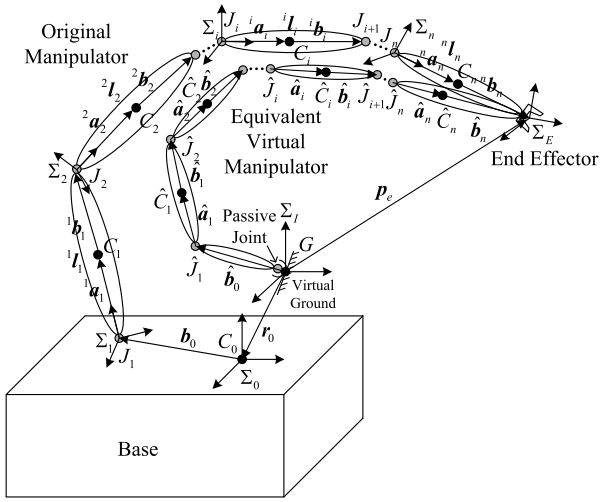

FIGURE 2. Equivalent VM of the n -DOF free-floating space manipulator.

m-dimensional space expanded by GCRV, and RS can be expressed as the following set

$$\boldsymbol{R} = \{\boldsymbol{\xi} \,|\, \boldsymbol{\xi} = [\xi_1, \xi_2, \cdots, \xi_m]^{\mathrm{T}},\ \xi_i^{\min} \le \xi_i \le \xi_i^{\max},\ i = 1, 2, \cdots, m\} \quad (2)$$

The GCRV that doesn't meet predefined constraints should be deleted, so the deleted GCRVs can make up some unreachable regions in RS. Introducing p constraints, i.e. $C_1, C_2, \cdots, C_p$, and assuming the unreachable region corresponds to a certain constraint C_i is $\boldsymbol{A}_{C_i}$, we obtain the unreachable regions in RS

$$\boldsymbol{A} = \bigcup_{i=1}^{p} \boldsymbol{A}_{C_i} \quad (3)$$

Deleting the unreachable regions $\boldsymbol{A}$, the reachable RS $\boldsymbol{R}_r$ can be obtained. It is the complementary set of $\boldsymbol{A}$

$$\boldsymbol{R}_r = \{\boldsymbol{\xi} \,|\, \boldsymbol{\xi} = [\xi_1, \xi_2, \cdots, \xi_m]^{\mathrm{T}} \notin \boldsymbol{A},\ \xi_i^{\min} \le \xi_i \le \xi_i^{\max},\ i = 1, 2, \cdots, m\} \quad (4)$$

The task execution process can be regarded as the transition of GCRV in $\boldsymbol{R}_r$. Based on $\boldsymbol{R}_r$, the criteria for task realizability is given

$$\begin{cases} (\boldsymbol{\xi}^0 \in \boldsymbol{R}_r) \cap (\boldsymbol{\xi}^d \in \boldsymbol{R}_r) \\ \forall \boldsymbol{\xi}^i \in \boldsymbol{R}_r, \boldsymbol{\xi}^i \in \{\boldsymbol{\xi}^0, \boldsymbol{\xi}^1, \cdots, \boldsymbol{\xi}^d\} \end{cases} \quad (5)$$

Eq.(5) can be described as

a The initial GCRV $\boldsymbol{\xi}^0$ and the desired GCRV $\boldsymbol{\xi}^d$ are both in $\boldsymbol{R}_r$

b The path connecting $\boldsymbol{\xi}^0$ and $\boldsymbol{\xi}^d$ exists, and all GCRVs on the path are all in $\boldsymbol{R}_r$. $\{\boldsymbol{\xi}^0, \boldsymbol{\xi}^1, \cdots, \boldsymbol{\xi}^d\}$ is the set of GCRVs on the connecting path.

For fixed-base manipulators, the assigned task is unrealizable if one of the conditions in Eq.(5) is not met. When the task is realizable, path planning is to find a path connecting $\boldsymbol{\xi}^0$ and $\boldsymbol{\xi}^d$ in $\boldsymbol{R}_r$, so $\boldsymbol{R}_r$ is known as a path planning domain.

For free-floating space manipulators, the base-coupled motion will influence task realizability and path planning, so the base-coupled motion characteristic must be considered in RS particularly. Therefore, we should select the representation variables that can reflect task attributes and base-coupled motion characteristic simultaneously. Generally speaking, the base-coupled motion is usually represented by $\boldsymbol{r}_0$ and $\boldsymbol{\Psi}_0$, because $\boldsymbol{r}_0$ and $\boldsymbol{\Psi}_0$ are unintegrable. If we know $\boldsymbol{r}_0$ and $\boldsymbol{\Psi}_0$ at every running moment, we can obtain base velocity $\boldsymbol{v}_0$ and $\boldsymbol{\omega}_0$, and base acceleration $\dot{\boldsymbol{v}}_0$ and $\dot{\boldsymbol{\omega}}_0$ correspondingly. Thus the representation variables of free-floating space manipulators should be related to $\boldsymbol{r}_0$ and $\boldsymbol{\Psi}_0$, and GCRV is expressed as:

$$\boldsymbol{\xi} = [\xi_1(\boldsymbol{x}_1, \boldsymbol{r}_0, \boldsymbol{\Psi}_0), \xi_2(\boldsymbol{x}_2, \boldsymbol{r}_0, \boldsymbol{\Psi}_0), \cdots, \xi_m(\boldsymbol{x}_m, \boldsymbol{r}_0, \boldsymbol{\Psi}_0)]^{\mathrm{T}} \in \mathbf{R}^m \quad (6)$$

$\boldsymbol{x}_1, \boldsymbol{x}_1, \cdots, \boldsymbol{x}_m$ are the manipulator system variables which are irrelevant to the base-coupled motion, i.e. $\boldsymbol{x}_i \ne f(\boldsymbol{r}_0, \boldsymbol{\Psi}_0)$, $i = 1, 2, \cdots, m$. Considering $\boldsymbol{r}_0 = \boldsymbol{r}_0(\boldsymbol{\theta}, \boldsymbol{\Psi}_0)$ (see Appendix Eq.(58)), GCRV becomes

$$\boldsymbol{\xi} = [\xi_1(\boldsymbol{x}_1, \boldsymbol{\theta}, \boldsymbol{\Psi}_0), \xi_2(\boldsymbol{x}_2, \boldsymbol{\theta}, \boldsymbol{\Psi}_0), \cdots, \xi_m(\boldsymbol{x}_m, \boldsymbol{\theta}, \boldsymbol{\Psi}_0)]^{\mathrm{T}} \in \mathbf{R}^m \quad (7)$$

Particularly, if $(\boldsymbol{\theta} \subseteq \boldsymbol{x}_1) \cap (\boldsymbol{\theta} \subseteq \boldsymbol{x}_2) \cap \cdots \cap (\boldsymbol{\theta} \subseteq \boldsymbol{x}_m)$, GCRV can be expressed as $\boldsymbol{\xi} = [\xi_1(\boldsymbol{x}_1, \boldsymbol{\Psi}_0), \xi_2(\boldsymbol{x}_2, \boldsymbol{\Psi}_0), \cdots, \xi_m(\boldsymbol{x}_m, \boldsymbol{\Psi}_0)]^{\mathrm{T}} \in \mathbf{R}^m$.

For example, aiming at the tasks in joint space, such as manipulator configuration fold and adjustment, $\boldsymbol{\theta}$ and $\boldsymbol{\Psi}_0$ are selected as representation variables. Thus RS is

$$\begin{aligned} \boldsymbol{R} = \{\boldsymbol{\xi} \,|\, & \boldsymbol{\xi} = [\boldsymbol{\theta}^{\mathrm{T}}, \boldsymbol{\Psi}_0^{\mathrm{T}}]^{\mathrm{T}},\ \boldsymbol{\theta} = [\theta_1, \theta_2, \cdots, \theta_n]^{\mathrm{T}}, \\ & \theta_i^{\min} \le \theta_i \le \theta_i^{\max},\ i = 1, 2, \cdots, n, \\ & \boldsymbol{\Psi}_0 = [\Psi_{0x}, \Psi_{0y}, \Psi_{0z}]^{\mathrm{T}},\ \boldsymbol{\Psi}_0 \in [\boldsymbol{\Psi}_0^{\min}, \boldsymbol{\Psi}_0^{\max}]\} \end{aligned} \quad (8)$$

where $\theta_i^{\min}$ and $\theta_i^{\max}$ are the lower and upper bounds of the i-th joint angle. $\boldsymbol{\Psi}_0 \in [\boldsymbol{\Psi}_0^{\min}, \boldsymbol{\Psi}_0^{\max}]$ denotes $\Psi_{0x}^{\min} \le \Psi_{0x} \le \Psi_{0x}^{\max}$, $\Psi_{0y}^{\min} \le \Psi_{0y} \le \Psi_{0y}^{\max}$, $\Psi_{0z}^{\min} \le \Psi_{0z} \le \Psi_{0z}^{\max}$, and $\Psi_{0x}^{\min}$, $\Psi_{0x}^{\max}$, $\Psi_{0y}^{\min}$, $\Psi_{0y}^{\max}$, $\Psi_{0z}^{\min}$, $\Psi_{0z}^{\max}$ are the theoretical reachable bounds of base attitude. They are usually set as $[\Psi_{0x}^{\min}, \Psi_{0x}^{\max}] = [\Psi_{0y}^{\min}, \Psi_{0y}^{\max}] = [\Psi_{0z}^{\min}, \Psi_{0z}^{\max}] = [-180°, 180°]$.

The space tasks in Cartesian space, such as space station assembly, spacecraft auxiliary docking, large load carrying, etc., hope the end-effector tracks the predefined path to arrive at desired position/attitude, so end-effector position/attitude are selected as representation variables. RS is

$$\begin{aligned} \boldsymbol{R} = \{\boldsymbol{\xi} | \boldsymbol{\xi} = [& x_e(\boldsymbol{\theta}, \boldsymbol{\Psi}_0), y_e(\boldsymbol{\theta}, \boldsymbol{\Psi}_0), z_e(\boldsymbol{\theta}, \boldsymbol{\Psi}_0), \\ & \alpha_e(\boldsymbol{\theta}, \boldsymbol{\Psi}_0), \beta_e(\boldsymbol{\theta}, \boldsymbol{\Psi}_0), \gamma_e(\boldsymbol{\theta}, \boldsymbol{\Psi}_0)]^{\mathrm{T}}\} \end{aligned} \quad (9)$$

Eq.(8) and Eq.(9) give the examples of selecting representation variables for RS aiming at the space tasks in joint space and Cartesian space. In fact, there is no fixed way to determine representation variables. We need to select the fewest independent representation variables according to the specific task and manipulator attributes.

To fully analyze the influences of base-coupled motion on task realizability and path planning, we classify RS into 5 types according to different base control modes. Then, we discuss effects of different types of RS on task realizability evaluation and path planning domain construction for free-floating space manipulators.

C. CLASSIFICATION OF RS ACCORDING TO BASE CONTROL MODES

For space manipulators, there are several base control modes, which mainly include "Fixed Base", "Attitude Constrained Base" and "Free-floating Base". In [15] and [19], Umetani *et al.* and Vafa *et al.* classified workspace of space manipulators according to different base control modes, and pointed out the variation of base attitude directly influences reachability of manipulators, and the task realizability will be further affected. According to different base control modes, we construct 5 types of RS for free-floating space manipulator: Fixed Vehicle RS (FRS), Attitude Constrained RS (CRS), Maximum Reachable RS (MRS), Guaranteed RS (GRS) and Partly Guaranteed RS (PGRS).

1) FRS

FRS is the RS of fixed-base space manipulators. In this case, $\boldsymbol{v}_0, \boldsymbol{\omega}_0$ and $\dot{\boldsymbol{v}}_0, \dot{\boldsymbol{\omega}}_0$ are zero, and base centroid position and base attitude are fixed, i.e. $\boldsymbol{r}_0 = \boldsymbol{r}_0^{\text{const}}$ and $\boldsymbol{\Psi}_0 = \boldsymbol{\Psi}_0^{\text{const}}$. The GCRV is

$$\boldsymbol{\xi} = [\xi_1(\boldsymbol{x}_1, \boldsymbol{r}_0^{\text{const}}, \boldsymbol{\Psi}_0^{\text{const}}), \xi_2(\boldsymbol{x}_2, \boldsymbol{r}_0^{\text{const}}, \boldsymbol{\Psi}_0^{\text{const}}), \cdots, \xi_m(\boldsymbol{x}_m, \boldsymbol{r}_0^{\text{const}}, \boldsymbol{\Psi}_0^{\text{const}})]^{\mathrm{T}} \in \mathbf{R}^m \quad (10)$$

FRS can be expressed as the following set

$$\begin{aligned}\boldsymbol{R}_{\text{FRS}} &= \{\boldsymbol{\xi} | \boldsymbol{\xi} \\ &= [\xi_1(\boldsymbol{x}_1, \boldsymbol{r}_0^{\text{const}}, \boldsymbol{\Psi}_0^{\text{const}}), \xi_2(\boldsymbol{x}_2, \boldsymbol{r}_0^{\text{const}}, \boldsymbol{\Psi}_0^{\text{const}}), \cdots, \\ &\quad \xi_m(\boldsymbol{x}_m, \boldsymbol{r}_0^{\text{const}}, \boldsymbol{\Psi}_0^{\text{const}})]^{\mathrm{T}}, \xi_{i\min} \le \xi_i \le \xi_{i\max}, \\ &\quad i = 1, 2, \cdots, m\} \end{aligned} \quad (11)$$

Deleting GCRVs which don't satisfy the predefined constraints, we can obtain the reachable FRS $\boldsymbol{R}_{\text{FRS}r}$. Based on the criteria for task realizability in Eq.(5), $\boldsymbol{R}_{\text{FRS}r}$ can only be utilized to evaluate task realizability and construct a path planning domain for the space manipulator whose base is fixed in $\boldsymbol{r}_0^{\text{const}}$ and $\boldsymbol{\Psi}_0^{\text{const}}$.

2) CRS

CRS is the RS when base attitude is fixed. In this case, $\boldsymbol{\omega}_0$ and $\dot{\boldsymbol{\omega}}_0$ are zero, and base attitude is fixed, i.e. $\boldsymbol{\Psi}_0 = \boldsymbol{\Psi}_0^{\text{const}}$. The linear momentum of system is conservative and integrable, so $\boldsymbol{r}_0 = \boldsymbol{r}_0(\boldsymbol{\theta}, \boldsymbol{\Psi}_0^{\text{const}})$. The GCRV is

$$\boldsymbol{\xi} = [\xi_1(\boldsymbol{x}_1, \boldsymbol{\theta}, \boldsymbol{\Psi}_0^{\text{const}}), \xi_2(\boldsymbol{x}_2, \boldsymbol{\theta}, \boldsymbol{\Psi}_0^{\text{const}}), \cdots, \xi_m(\boldsymbol{x}_m, \boldsymbol{\theta}, \boldsymbol{\Psi}_0^{\text{const}})]^{\mathrm{T}} \in \mathbf{R}^m \quad (12)$$

If $(\boldsymbol{\theta} \subseteq \boldsymbol{x}_1) \cap (\boldsymbol{\theta} \subseteq \boldsymbol{x}_2) \cap \cdots \cap (\boldsymbol{\theta} \subseteq \boldsymbol{x}_m)$, GCRV becomes $\boldsymbol{\xi} = [\xi_1(\boldsymbol{x}_1, \boldsymbol{\Psi}_0^{\text{const}}), \xi_2(\boldsymbol{x}_2, \boldsymbol{\Psi}_0^{\text{const}}), \cdots, \xi_m(\boldsymbol{x}_m, \boldsymbol{\Psi}_0^{\text{const}})]^{\mathrm{T}} \in \boldsymbol{R}^m$.

CRS can be expressed as the following set

$$\begin{aligned}\boldsymbol{R}_{\text{CRS}} &= \{\boldsymbol{\xi} | \boldsymbol{\xi} = [\xi_1(\boldsymbol{x}_1, \boldsymbol{\theta}, \boldsymbol{\Psi}_0^{\text{const}}), \xi_2(\boldsymbol{x}_2, \boldsymbol{\theta}, \boldsymbol{\Psi}_0^{\text{const}}), \cdots, \\ &\quad \xi_m(\boldsymbol{x}_m, \boldsymbol{\theta}, \boldsymbol{\Psi}_0^{\text{const}})]^{\mathrm{T}}, \xi_{i\min} \le \xi_i \le \xi_{i\max}, \\ &\quad i = 1, 2, \cdots, m\} \end{aligned} \quad (13)$$

The CRS corresponding to base attitude fixed in $\boldsymbol{\Psi}_0$ is expressed as $\boldsymbol{R}_{\text{CRS}}^{\boldsymbol{\Psi}_0}$. Considering some predefined constraints, we can obtain reachable CRS $\boldsymbol{R}_{\text{CRS}r}^{\boldsymbol{\Psi}_0}$. Utilizing Eq.(5) in $\boldsymbol{R}_{\text{CRS}r}^{\boldsymbol{\Psi}_0}$, we can only check the task realizability and construct a path planning domain for the space manipulator whose base attitude is fixed in $\boldsymbol{\Psi}_0$.

As can be seen from Eq.(12)-(13), CRS depends on $\boldsymbol{\Psi}_0$ instead of $\boldsymbol{R}_0$. In other words, for different base attitudes, we can obtain different collections of reachable representation variables. Therefore, the base attitude $\boldsymbol{\Psi}_0$ (instead of base centroid position $\boldsymbol{R}_0$) mainly influences task realizability and path planning of free-floating space manipulators. Correspondingly, base attitudes that allow space manipulator to reach a certain known GCRV $\boldsymbol{\xi}$ will form a range. Therefore, in path planning, we must particularly consider the control of coupled motion of base attitude.

CRS reveals the influences of variation of base attitude on task realizability and path planning. And the task realizablity evaluation and path planning domain construction of free-floating space manipulators must be based on CRS.

3) MRS

MRS is the RS that consists of all theoretically reachable representation variables of free-floating space manipulator. In this case, base attitude freely varies in a theoretical reachable range, i.e. $\boldsymbol{\Psi}_0 \in [\boldsymbol{\Psi}_0^{\min}, \boldsymbol{\Psi}_0^{\max}]$. System momentum is conservative, so $\boldsymbol{r}_0 = \boldsymbol{r}_0(\boldsymbol{\theta}, \boldsymbol{\Psi}_0)$. The GCRV is

$$\boldsymbol{\xi} = [\xi_1(\boldsymbol{x}_1, \boldsymbol{\theta}, \boldsymbol{\Psi}_0), \xi_2(\boldsymbol{x}_2, \boldsymbol{\theta}, \boldsymbol{\Psi}_0), \cdots, \xi_m(\boldsymbol{x}_m, \boldsymbol{\theta}, \boldsymbol{\Psi}_0)]^{\mathrm{T}} \in \mathbf{R}^m \quad (14)$$

If $(\boldsymbol{\theta} \subseteq \boldsymbol{x}_1) \cap (\boldsymbol{\theta} \subseteq \boldsymbol{x}_2) \cap \cdots \cap (\boldsymbol{\theta} \subseteq \boldsymbol{x}_m)$, GCRV is $\boldsymbol{\xi} = [\xi_1(\boldsymbol{x}_1, \boldsymbol{\Psi}_0), \xi_2(\boldsymbol{x}_2, \boldsymbol{\Psi}_0), \cdots, \xi_m(\boldsymbol{x}_m, \boldsymbol{\Psi}_0)]^{\mathrm{T}} \in \boldsymbol{R}^m$.

MRS can be expressed as the following set

$$\begin{aligned}\boldsymbol{R}_{\text{MRS}} &= \{\boldsymbol{\xi} | \boldsymbol{\xi} = [\xi_1(\boldsymbol{x}_1, \boldsymbol{\theta}, \boldsymbol{\Psi}_0), \xi_2(\boldsymbol{x}_2, \boldsymbol{\theta}, \boldsymbol{\Psi}_0), \cdots, \\ &\quad \xi_m(\boldsymbol{x}_m, \boldsymbol{\theta}, \boldsymbol{\Psi}_0)]^{\mathrm{T}}, \ \xi_i^{\min} \le \xi_i \le \xi_i^{\max}, \\ &\quad i = 1, 2, \cdots, m \boldsymbol{\Psi}_0 \in [\boldsymbol{\Psi}_0^{\min}, \boldsymbol{\Psi}_0^{\max}]\} \end{aligned} \quad (15)$$

From Eq.(14)-(15) and Eq.(12)-(13), base attitude for CRS is fixed in a certain value in $[\boldsymbol{\Psi}_0^{\min}, \boldsymbol{\Psi}_0^{\max}]$, and base attitude for MRS freely varies in $[\boldsymbol{\Psi}_0^{\min}, \boldsymbol{\Psi}_0^{\max}]$. Thus MRS is equivalent to a union of all CRS corresponding to base attitude traversing in $[\boldsymbol{\Psi}_0^{\min}, \boldsymbol{\Psi}_0^{\max}]$, i.e.

$$\boldsymbol{R}_{\text{MRS}} = \bigcup_{\boldsymbol{\Psi}_0 \in [\boldsymbol{\Psi}_0^{\min}, \boldsymbol{\Psi}_0^{\max}]} \boldsymbol{R}_{\text{CRS}}^{\boldsymbol{\Psi}_0} \quad (16)$$

Considering some predefined constraints, we can obtain reachable MRS $\boldsymbol{R}_{\text{MRS}r}$

$$\boldsymbol{R}_{\text{MRS}r} = \bigcup_{\boldsymbol{\Psi}_0 \in [\boldsymbol{\Psi}_0^{\min}, \boldsymbol{\Psi}_0^{\max}]} \boldsymbol{R}_{\text{CRS}r}^{\boldsymbol{\Psi}_0} \quad (17)$$

MRS is constructed with all theoretically reachable representation variables of free-floating space manipulators, and it entirely neglects the reachability of base attitude at all. Utilizing Eq.(5) in $\boldsymbol{R}_{\mathrm{MRS}r}$, we can easily know even if two conditions are both satisfied, the task may not be realizable, because base attitudes of some GCRVs in the searched path may not be reachable. But if task is realizable, the two conditions must be satisfied. Therefore, Eq.(5) in MRS is only the necessary condition for that the task is realizable. We can't use it to check task realizability and construct a path planning domain for free-floating space manipulators.

4) GRS

GRS is the RS consisting of the representation variables whose reachable base attitude range equals to the theoretical reachable range. The GCRV is same with Eq.(14). Mathematically, GRS is equivalent to an intersection of all CRS corresponding to base attitude traversing in $[\boldsymbol{\Psi}_0^{\min}, \boldsymbol{\Psi}_0^{\max}]$, i.e.

$$\boldsymbol{R}_{\mathrm{GRS}} = \bigcap_{\boldsymbol{\Psi}_0 \in [\boldsymbol{\Psi}_0^{\min}, \boldsymbol{\Psi}_0^{\max}]} \boldsymbol{R}_{\mathrm{CRS}}^{\boldsymbol{\Psi}_0} \tag{18}$$

Considering some predefined constraints, we can obtain the reachable GRS

$$\boldsymbol{R}_{\mathrm{GRS}r} = \bigcap_{\boldsymbol{\Psi}_0 \in [\boldsymbol{\Psi}_0^{\min}, \boldsymbol{\Psi}_0^{\max}]} \boldsymbol{R}_{\mathrm{CRS}r}^{\boldsymbol{\Psi}_0} \tag{19}$$

Because the reachable base attitude ranges of all representation variables in GRS equals to $[\boldsymbol{\Psi}_0^{\min}, \boldsymbol{\Psi}_0^{\max}]$, free-floating space manipulators can track the path in GRS to perform task without controlling base-coupled motion, so GRS is an ideal path planning domain in a sense. However, for the theoretical range $\Psi_{0x} \in [-180°, 180°]$, $\Psi_{0y} \in [-180°, 180°]$, $\Psi_{0z} \in [-180°, 180°]$. GRS may be very small or even empty, so path planning in GRS is prone to fail.

Utilizing Eq.(5) in $\boldsymbol{R}_{\mathrm{GRS}r}$, we can find if two conditions are both satisfied, the task must be realizable. But path planning fails in GRS, or GRS is empty doesn't means the task is unrealizable, but the condition that base attitude is fully reachable is too strict. Thus Eq.(5) is only the sufficient condition for that the task is realizable. In practice, to guarantee the system stability and solar collection efficiency, base attitude deflection must be always limited in a certain range when space manipulators perform tasks, i.e. ${}^{\mathrm{allow}}\boldsymbol{\Psi}_0 \in [{}^{\mathrm{allow}}\boldsymbol{\Psi}_0^{\min}, {}^{\mathrm{allow}}\boldsymbol{\Psi}_0^{\max}]$, and $[{}^{\mathrm{allow}}\boldsymbol{\Psi}_0^{\min}, {}^{\mathrm{allow}}\boldsymbol{\Psi}_0^{\max}] \subset [\boldsymbol{\Psi}_0^{\min}, \boldsymbol{\Psi}_0^{\max}]$. Therefore, GRS considers the control of base-coupled motion in excess, so it is underemployed for task realizability evaluation and path planning domain construction. Therefore, we need to construct a new kind of RS with appropriate consideration of the practical base attitude deflection limitation.

5) PGRS

Considering the practical base attitude deflection limitation, we construct PGRS. To ensure that PGRS contains $\boldsymbol{\xi}^0$ and $\boldsymbol{\xi}^d$, we calculate the reachable base attitude ranges of $\boldsymbol{\xi}^0$ and $\boldsymbol{\xi}^d$. Intersecting them with the practical base attitude deflection limitation, we obtain the practical reachable range of base attitude $\boldsymbol{\Psi}_0 \in [\boldsymbol{\Psi}_0^{\mathrm{lower}}, \boldsymbol{\Psi}_0^{\mathrm{upper}}]$. PGRS consists of the representation variables whose reachable base attitude ranges cover the practical reachable range $\boldsymbol{\Psi}_0 \in [\boldsymbol{\Psi}_0^{\mathrm{lower}}, \boldsymbol{\Psi}_0^{\mathrm{upper}}]$. In other words, PGRS corresponds to an intersection of all CRS corresponding to base attitude traversing in $[\boldsymbol{\Psi}_0^{\mathrm{lower}}, \boldsymbol{\Psi}_0^{\mathrm{upper}}]$. When free-floating space manipulators track the path in PGRS, we need to limit base attitude in the practical reachable range through non-holonomic motion planning method [10].

The construction of PGRS is described as follow:

Step 1: Judging the inclusions of $\boldsymbol{\xi}^0$ and $\boldsymbol{\xi}^d$ in all CRS corresponding to base attitude traversing in $[\boldsymbol{\Psi}_0^{\min}, \boldsymbol{\Psi}_0^{\max}]$, the reachable base attitude ranges of $\boldsymbol{\xi}^0$ and $\boldsymbol{\xi}^d$ can be obtained: ${}^{\xi^0}\boldsymbol{\Psi}_0 \in [{}^{\xi^0}\boldsymbol{\Psi}_0^{\min}, {}^{\xi^0}\boldsymbol{\Psi}_0^{\max}]$ and ${}^{\xi^d}\boldsymbol{\Psi}_0 \in [{}^{\xi^d}\boldsymbol{\Psi}_0^{\min}, {}^{\xi^d}\boldsymbol{\Psi}_0^{\max}]$.

Step 2: To ensure that PGRS contains $\boldsymbol{\xi}^0$ and $\boldsymbol{\xi}^d$, and meets base attitude deflection limitation, we obtain the practical reachable range of base attitude $[\boldsymbol{\Psi}_0^{\mathrm{lower}}, \boldsymbol{\Psi}_0^{\mathrm{upper}}]$ through intersecting $[{}^{\xi^0}\boldsymbol{\Psi}_0^{\min}, {}^{\xi^0}\boldsymbol{\Psi}_0^{\max}]$, $[{}^{\xi^d}\boldsymbol{\Psi}_0^{\min}, {}^{\xi^d}\boldsymbol{\Psi}_0^{\max}]$, and $[{}^{\mathrm{allow}}\boldsymbol{\Psi}_0^{\min}, {}^{\mathrm{allow}}\boldsymbol{\Psi}_0^{\max}]$

$$\begin{aligned}[\boldsymbol{\Psi}_0^{\mathrm{lower}}, \boldsymbol{\Psi}_0^{\mathrm{upper}}] = {} & [{}^{\xi^0}\boldsymbol{\Psi}_0^{\min}, {}^{\xi^0}\boldsymbol{\Psi}_0^{\max}] \cap [{}^{\xi^d}\boldsymbol{\Psi}_0^{\min}, {}^{\xi^d}\boldsymbol{\Psi}_0^{\max}] \\ & \cap [{}^{\mathrm{allow}}\boldsymbol{\Psi}_0^{\min}, {}^{\mathrm{allow}}\boldsymbol{\Psi}_0^{\max}]\end{aligned} \tag{20}$$

Step 3: Calculating the intersection of all CRS corresponding to base attitude traversing in $[\boldsymbol{\Psi}_0^{\mathrm{lower}}, \boldsymbol{\Psi}_0^{\mathrm{upper}}]$, we obtain PGRS

$$\boldsymbol{R}_{\mathrm{PGRS}} = \bigcap_{\boldsymbol{\Psi}_0 \in [\boldsymbol{\Psi}_0^{\mathrm{lower}}, \boldsymbol{\Psi}_0^{\mathrm{upper}}]} \boldsymbol{R}_{\mathrm{CRS}}^{\boldsymbol{\Psi}_0} \tag{21}$$

Considering some predefined constraints, we obtain reachable PGRS

$$\boldsymbol{R}_{\mathrm{PGRS}r} = \bigcap_{\boldsymbol{\Psi}_0 \in [\boldsymbol{\Psi}_0^{\mathrm{lower}}, \boldsymbol{\Psi}_0^{\mathrm{upper}}]} \boldsymbol{R}_{\mathrm{CRS}r}^{\boldsymbol{\Psi}_0} \tag{22}$$

Because $[\boldsymbol{\Psi}_0^{\mathrm{lower}}, \boldsymbol{\Psi}_0^{\mathrm{upper}}] \subset [\boldsymbol{\Psi}_0^{\min}, \boldsymbol{\Psi}_0^{\max}]$, for the same representation variables, PGRS is obviously bigger than GRS. Moreover, the reachable base attitude ranges of all GCRVs in PGRS must be equal or greater than the practical reachable range of base attitude $[\boldsymbol{\Psi}_0^{\mathrm{lower}}, \boldsymbol{\Psi}_0^{\mathrm{upper}}]$, so when space manipulators track the path in PGRS, we only need to limit base attitude in $[\boldsymbol{\Psi}_0^{\mathrm{lower}}, \boldsymbol{\Psi}_0^{\mathrm{upper}}]$ through non-holonomic motion planning method. And Eq.(5) in PGRS is the sufficient and necessary condition that the task is realizable for the free-floating space manipulator whose base attitude should be limited in $[\boldsymbol{\Psi}_0^{\mathrm{lower}}, \boldsymbol{\Psi}_0^{\mathrm{upper}}]$. Therefore, PGRS can be applied to check task realizability and construct a path planning domain for free-floating space manipulators. Particularly, the criteria for task realizability in PGRS can be given as follow

$$\begin{cases} (\boldsymbol{\xi}^0 \in \boldsymbol{R}_{\mathrm{PGRS}r}^{[\boldsymbol{\Psi}_0^{\mathrm{lower}}, \boldsymbol{\Psi}_0^{\mathrm{upper}}]}) \cap (\boldsymbol{\xi}^d \in \boldsymbol{R}_{\mathrm{PGRS}r}^{[\boldsymbol{\Psi}_0^{\mathrm{lower}}, \boldsymbol{\Psi}_0^{\mathrm{upper}}]}) \\ \forall \boldsymbol{\xi}^i \in \boldsymbol{R}_{\mathrm{PGRS}r}^{[\boldsymbol{\Psi}_0^{\mathrm{lower}}, \boldsymbol{\Psi}_0^{\mathrm{upper}}]}, \boldsymbol{\xi}^i \in \{\boldsymbol{\xi}^0, \cdots, \boldsymbol{\xi}^i, \cdots, \boldsymbol{\xi}^d\} \end{cases} \tag{23}$$

where $\boldsymbol{R}_{\mathrm{PGRS}r}^{[\boldsymbol{\Psi}_0^{\mathrm{lower}}, \boldsymbol{\Psi}_0^{\mathrm{upper}}]}$ is the PGRS corresponding to base attitude is required to be limited in the practical reachable range of base attitude $[\boldsymbol{\Psi}_0^{\mathrm{lower}}, \boldsymbol{\Psi}_0^{\mathrm{upper}}]$. The criteria in Eq.(23) illustrates that the task will be realizable, only if the reachable PGRS contains both initial and desired GCRVs, and the path connecting them exists.

D. DISCUSSION OF DIFFERENT TYPES OF RS

Based on different base control modes, we give 5 types of RS for space manipulators. According to the definitions of different types of RS, and for the same representation variables, we have following relationships among CRS, MRS, GRS, and PGRS

$$\begin{aligned} &\boldsymbol{R}_{\mathrm{GRS}} \subseteq \boldsymbol{R}_{\mathrm{CRS}}^{\boldsymbol{\Psi}_0} \subseteq \boldsymbol{R}_{\mathrm{MRS}} \ \text{ if } \boldsymbol{\Psi}_0 \in [\boldsymbol{\Psi}_0^{\min}, \boldsymbol{\Psi}_0^{\max}] \\ &\boldsymbol{R}_{\mathrm{GRS}} \subseteq \boldsymbol{R}_{\mathrm{CRS}}^{\boldsymbol{\Psi}_0} \subseteq \boldsymbol{R}_{\mathrm{CRS}}^{\boldsymbol{\Psi}_0} \subseteq \boldsymbol{R}_{\mathrm{MRS}} \ \text{ if } \boldsymbol{\Psi}_0 \in [\boldsymbol{\Psi}_0^{\mathrm{lower}}, \boldsymbol{\Psi}_0^{\mathrm{upper}}] \end{aligned} \tag{24}$$

Different types of RS have different effects on task realizability evaluation and path planning domain construction for space manipulators:

a) FRS is only appropriate for evaluating task realizability and constructing a path planning domain for the manipulator whose base is fixed in current position/attitude, so it is inapplicable for free-floating space manipulators.

b) CRS limits base attitude, so it is inapplicable for free-floating space manipulators, either. But CRS illustrates that different base attitudes produce different reachable representation variables, so the variation of base attitude will directly influence task realizability and path planning of free-floating space manipulators. On the contrary, for the known GCRV, its reachable base attitudes will form a range, so we must consider the control of coupled motion of base attitude in path planning.

c) MRS is a union of all CRS corresponding to base attitude fixed in the theoretical reachable range. MRS is constructed with all reachable representation variables of free-floating space manipulators, but it doesn't consider the control of base-coupled motion. Eq.(5) in MRS is only the necessary condition for that the task is realizable. We can't check task realizability and search path in it.

d) GRS is an intersection of all CRS corresponding to base attitude fixed in the theoretical reachable range, so base attitude of representation variables in GRS is completely reachable. Free-floating space manipulators can track the path in GRS to successfully complete task even without extra control of the base motion, so GRS is an ideal path planning domain in a sense. But because the condition that base attitude is fully reachable is too strict, GRS is usually small or even empty, and path planning in GRS may easily fail. In practice, the base attitude deflection is always limited, so GRS is underemployed for path planning. Moreover, Eq.(5) in GRS is only the sufficient condition for that the task is realizable. Thus we shouldn't use GRS to plan path and check task realizability for free-floating space manipulators.

e) To satisfy the base attitude deflection limitation, we construct PGRS according to the practical reachable range of base attitude, and the path planning domain is expanded. PGRS can be applied to check task realizability and construct a path planning domain for free-floating space manipulators.

Classifying RS of free-floating space manipulators into 5 different types can help us understand the effects of base-coupled motion on task realizability and path planning of space manipulator. Although FRS and CRS are not applicable to free-floating space manipulator, they are the basis of constructing MRS, GRS and PGRS. In a word, the classification of RS for space manipulator is reasonable.

Task realizability evaluation and path planning domain construction for free-floating space manipulators can be expressed as: Selecting can that reflect task attributes and are relative to $\boldsymbol{r}_0$ and $\boldsymbol{\Psi}_0$, all reachable CRS corresponding to base attitude fixed in $[\boldsymbol{\Psi}_0^{\min}, \boldsymbol{\Psi}_0^{\max}]$ are constructed at first. Then, we calculate the practical reachable range of base attitude and obtain the reachable PGRS. Utilizing Eq.(5), task realizability can be checked in the reachable PGRS. And the reachable PGRS can serve as a path planning domain for free-floating space manipulators. Finally, path planning can be conducted in the reachable PGRS.

III. PATH PLANNING IN REPRESENTATION SPACE

We utilize A* algorithm to search path in PGRS. A* algorithm is a heuristic search algorithm which can find the shortest straight path connecting the initial and desired states for the realizable task, and it isn't affected by the dimensionality of planning domain. All the points on the obtained path are reachable without any doubt because A* algorithm can avoid unreachable regions automatically. The space in which A* algorithm searches path should be made up of the uniformly distributing grids. Then A* algorithm uses the cost function $f(\mathrm{gird}_i) = g(\mathrm{gird}_i) + h(\mathrm{gird}_i)$ as path search index in current gird_i, where $g(\mathrm{gird}_i)$ denotes the cost from the initial grid to gird_i, and $h(\mathrm{gird}_i)$ denotes the cost from gird_i to the target grid, $f(\mathrm{gird}_i)$ is the total cost. The cost is usually selected as distance. For the unreachable grid, its total cost is infinite, so they will be avoided automatically. Comparing all the costs of grids around gird_i, we obtain the grid with the lowest total cost as the next grid. Path searching will not be finished until the target grid is arrived, and the path consists of center points of the selected grids. Some of the adjacent center points on the same line can form a segment, so the path searched by A* algorithm consists of several straight segments.

In fact, we can also plan a more complicated path through other searching method, such as PRM algorithm, RRT algorithm, and so on, but in this paper, we mainly aim to explaining that we can find the executable task path in RS, so without loss of generality, we choose to utilize the classic A* algorithm to search the reachable straight path.

We give the detailed procedure of path planning in PGRS.

Step 1: Discretizing the theoretical reachable range of base attitude $\Psi_{0x} \in [\Psi_{0x}^{\min}, \Psi_{0x}^{\max}]$, $\Psi_{0y} \in [\Psi_{0y}^{\min}, \Psi_{0y}^{\max}]$ and

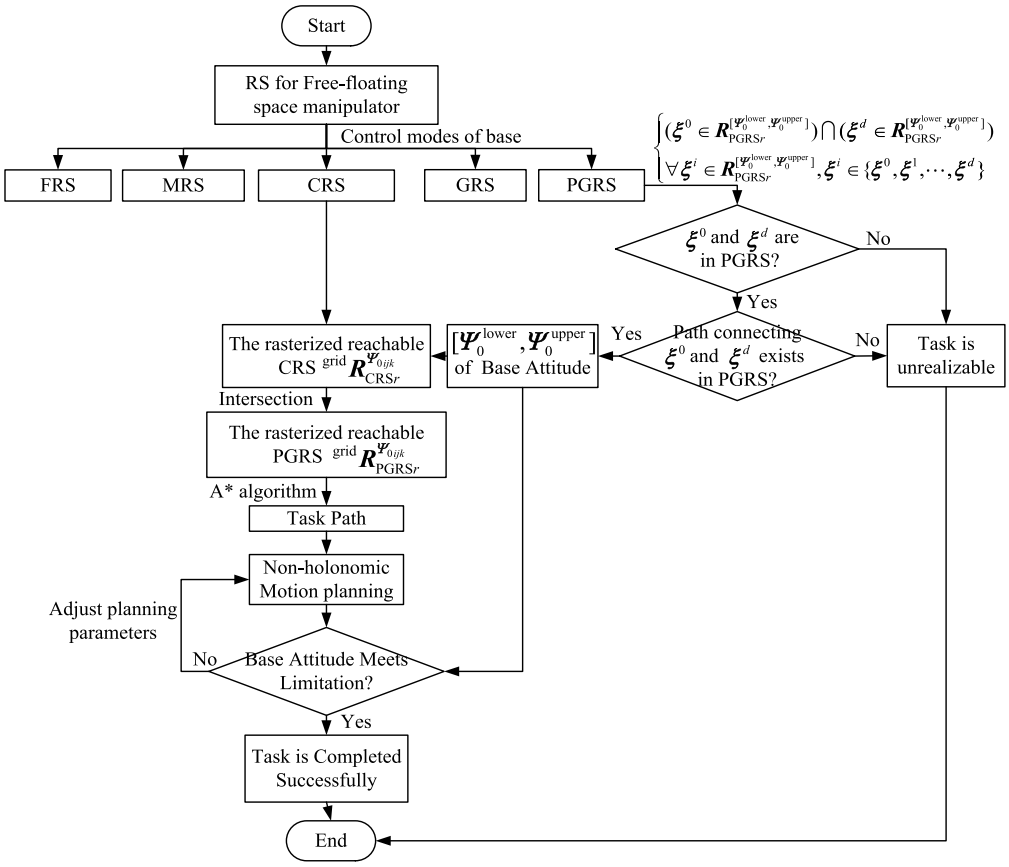

FIGURE 3. The procedure of path planning based on RS analytical method for free-floating space manipulators.

$\Psi_{0z} \in [\Psi_{0z}^{\min}, \Psi_{0z}^{\max}]$ by $\Delta\Psi_0$, we have $n_x = (\Psi_{0x}^{\max} - \Psi_{0x}^{\min})/\Delta\Psi_0$, $n_y = (\Psi_{0y}^{\max} - \Psi_{0y}^{\min})/\Delta\Psi_0$, $n_z = (\Psi_{0z}^{\max} - \Psi_{0z}^{\min})/\Delta\Psi_0$ base attitudes in x-axis, y-axis, and in z-axis.

Step 2: Traversing the discretized base attitudes, we obtain the theoretical reachable base attitudes set

$$\begin{aligned}\boldsymbol{\Psi}_{0\_\mathrm{theor}} = \{\boldsymbol{\Psi}_{0ijk} | \boldsymbol{\Psi}_{0ijk} = [\Psi_{0x}^{\min} + i \cdot \Delta\Psi_0, \Psi_{0y}^{\min} \\ + j \cdot \Delta\Psi_0, \Psi_{0z}^{\min} + k \cdot \Delta\Psi_0]^{\mathrm{T}}, i = 0, 1, \cdots, n_x, \\ j = 0, 1, \cdots, n_y, k = 0, 1, \cdots, n_z\} \end{aligned} \tag{25}$$

Then we obtain reachable CRS set corresponding to the theoretical reachable base attitude range: $\mathbf{R}_{\mathrm{CRS}r}^{\mathrm{theor}} = \{\boldsymbol{R}_{\mathrm{CRS}r}^{\boldsymbol{\Psi}_{0ijk}} | \boldsymbol{\Psi}_{0ijk} \in \boldsymbol{\Psi}_{0\_\mathrm{theor}}\}$.

Step 3: Before searching path, we must rasterize RS into the uniformly distributing grids. Utilizing the m-dimensional cuboid whose side length is $a_1, a_2, \cdots, a_m$ to envelope CRS. The surfaces of the cuboid are perpendicular to axes of the m-dimensional rectangular coordinate frame, and intersect coordinate axis ξ_1 at $(a_1/2, 0, \cdots, 0)^{\mathrm{T}}$ and $(-a_1/2, 0, \cdots, 0)^{\mathrm{T}}$, intersect coordinate axis ξ_2 at $(0, a_2/2, \cdots, 0)^{\mathrm{T}}$ and $(0, -a_2/2, \cdots, 0)^{\mathrm{T}}$,..., intersect coordinate axis ξ_m at $(0, \cdots, 0, a_m/2)^{\mathrm{T}}$ and $(0, \cdots, 0, -a_m/2)^{\mathrm{T}}$. We rasterize big cuboid into grids whose side length is $a_{g1}, a_{g2}, \cdots, a_{gm}$. Then for a known GCRV $\boldsymbol{\xi}^{\boldsymbol{\Psi}_{0ijk}} = [\xi_1^{\boldsymbol{\Psi}_{0ijk}}, \xi_2^{\boldsymbol{\Psi}_{0ijk}}, \cdots, \xi_m^{\boldsymbol{\Psi}_{0ijk}}]^{\mathrm{T}}$ in $\boldsymbol{R}_{\mathrm{CRS}r}^{\boldsymbol{\Psi}_{0ijk}}$, it belongs to the grid whose central point coordinates are

$$\begin{aligned}&[{}^{\mathrm{grid}}\xi_1^{\boldsymbol{\Psi}_{0ijk}}, {}^{\mathrm{grid}}\xi_2^{\boldsymbol{\Psi}_{0ijk}}, \cdots, {}^{\mathrm{grid}}\xi_m^{\boldsymbol{\Psi}_{0ijk}}]^{\mathrm{T}} \\ &= \left[\frac{-a_1 + (2s_1 - 1)a_{g1}}{2}, \frac{-a_2 + (2s_2 - 1)a_{g2}}{2}, \cdots, \right. \\ &\qquad \left. \frac{-a_m + (2s_m - 1)a_{gm}}{2}\right]^{\mathrm{T}} \end{aligned} \tag{26}$$

where $s_i = \min\left(\left\lfloor \frac{\xi_i^{\boldsymbol{\Psi}_{0ijk}} + a_1/2}{a_{gi}} \right\rfloor + 1, \left\lfloor \frac{a_i}{a_{gi}} \right\rfloor + 1\right), i = 1, 2, \cdots, m$.

Recording all central point coordinates of the grids which contain the representation variables, the reachable CRS is rasterized as ${}^{\mathrm{grid}}\boldsymbol{R}_{\mathrm{CRS}r}^{\boldsymbol{\Psi}_{0ijk}}$. Traversing all $\boldsymbol{R}_{\mathrm{CRS}r}^{\boldsymbol{\Psi}_{0ijk}}$ in $\mathbf{R}_{\mathrm{CRS}r}^{\mathrm{theor}}$, we have the rasterized reachable CRS set ${}^{\mathrm{grid}}\mathbf{R}_{\mathrm{CRS}}^{\mathrm{theor}} = \{{}^{\mathrm{grid}}\boldsymbol{R}_{\mathrm{CRS}}^{\boldsymbol{\Psi}_{0ijk}} | \boldsymbol{\Psi}_{0ijk} \in \boldsymbol{\Psi}_{0\_\mathrm{theor}}\}$.

Step 4: Practical reachable range of base attitude is calculated by Eq.(20). Screening out all reachable CRS whose base attitude traversing in $[\boldsymbol{\Psi}_0^{\mathrm{lower}}, \boldsymbol{\Psi}_0^{\mathrm{upper}}]$, we have ${}^{\mathrm{grid}}\mathbf{R}_{\mathrm{CRS}}^{\mathrm{prac}} = \{{}^{\mathrm{grid}}\boldsymbol{R}_{\mathrm{CRS}}^{\boldsymbol{\Psi}_{0ijk}} | \boldsymbol{\Psi}_{0ijk} \in [\boldsymbol{\Psi}_0^{\mathrm{lower}}, \boldsymbol{\Psi}_0^{\mathrm{upper}}]\}$.

Step 5: The intersection of all ${}^{\mathrm{grid}}\boldsymbol{R}_{\mathrm{CRS}}^{\boldsymbol{\Psi}_{0ijk}}$ is ${}^{\mathrm{grid}}\boldsymbol{R}_{\mathrm{PGRS}}$, and we can search path in the reachable PGRS ${}^{\mathrm{grid}}\boldsymbol{R}_{\mathrm{PGRS}}$ through A* algorithm.

The procedure of path planning based on the RS analytical method for free-floating space manipulators is in Fig.3.

The RS analytical method builds the direct connection between manipulator system variables and task attributes. For different tasks, we only need to select appropriate representation variables connected to task requirements, so the RS analytical method is universal for path planning of space manipulator performing various space tasks.

To ensure the task can be successfully completed, we should always limit base attitude in $[\boldsymbol{\Psi}_0^{\text{lower}}, \boldsymbol{\Psi}_0^{\text{upper}}]$ when space manipulators track path in PGRS, which can be achieved by non-holonomic motion planning [10]. To help readers understand RS easily, we apply the RS analytical method and path planning strategy to the 3-DOF free-floating space manipulator, and design a path tracking strategy based on non-holonomic motion planning in the next section.

IV. AN EXAMPLE OF THE 3-DOF FREE-FLOATING SPACE MANIPULATOR

Theoretically, the RS analytical method can be applied to space manipulators with arbitrary DOFs, but for high-DOF space manipulators, dimensionality of RS is so high that RS can't be drawn. For example, the dimensionalities of RS in Eq.(8) and Eq.(9) are n and 6 respectively, so we can't draw them. To help readers easily understand the RS analytical method for free-floating space manipulators, we take the 3-DOF free-floating space manipulator as an example to visually show RS. Aiming at the end-effector transferring task requiring end-effector to track the predefined path to desired position/attitude, we select end-effector position/attitude as representation variables to construct RS for path planning. Finally, we design a non-holonomic motion planning strategy to keep base attitude within the practical reachable range when manipulators track the path to perform task.

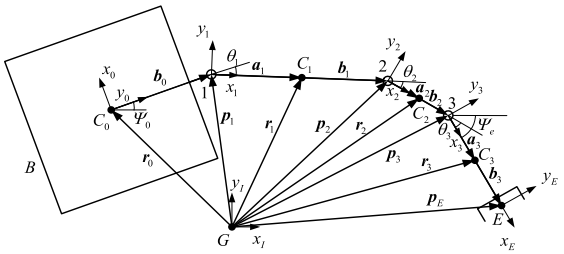

FIGURE 4. Kinematics model of 3-DOF free-floating space manipulator.

A. The EQUIVALENT VM of 3-DOF FREE-FLOATING SPACE MANIPULATOR

Fig.4 shows the kinematics model of 3-DOF free-floating space manipulator.

The inertial coordinate frame is established in centroid of the manipulator system. According to Eq.(1), end-effector position/attitude are

$$\begin{aligned}\boldsymbol{p}_e &= \frac{m_0}{M}\boldsymbol{b}_0 + \left(\frac{m_0}{M}\boldsymbol{a}_1 + \frac{m_0+m_1}{M}\boldsymbol{b}_1\right) \\ &+ \left(\frac{m_0+m_1}{M}\boldsymbol{a}_2 + \frac{m_0+m_1+m_2}{M}\boldsymbol{b}_2\right) \\ &+ \left(\frac{m_0+m_1+m_2}{M}\boldsymbol{a}_3 + \boldsymbol{b}_3\right) \\ &= \hat{\boldsymbol{b}}_0 + \sum_{i=1}^{3}(\hat{\boldsymbol{a}}_i + \hat{\boldsymbol{b}}_i) \\ &= \hat{\boldsymbol{b}}_0 + \hat{\boldsymbol{l}}_1 + \hat{\boldsymbol{l}}_2 + \hat{\boldsymbol{l}}_3 \\ &= \begin{bmatrix} \hat{b}_0\cos\Psi_0^{\text{const}} + \hat{l}_1 c_{01} + \hat{l}_2 c_{012} + \hat{l}_3 c_{0123} \\ \hat{b}_0\sin\Psi_0^{\text{const}} + \hat{l}_1 s_{01} + \hat{l}_2 s_{012} + \hat{l}_3 s_{0123} \end{bmatrix} \quad (27)\end{aligned}$$

$$\Psi_e = \Psi_0 + \theta_1 + \theta_2 + \theta_3 \quad (28)$$

where $\hat{b}_0$, $\hat{l}_1$, $\hat{l}_2$ and $\hat{l}_3$ are norms of $\hat{\boldsymbol{b}}_0$, $\hat{\boldsymbol{l}}_1$, $\hat{\boldsymbol{l}}_2$ and $\hat{\boldsymbol{l}}_3$, $c_{0ijk} = \cos(\Psi_0 + \theta_i + \theta_j + \theta_k)$, $s_{0ijk} = \sin(\Psi_0 + \theta_i + \theta_j + \theta_k)$.

The equivalent VM is in Fig.5.

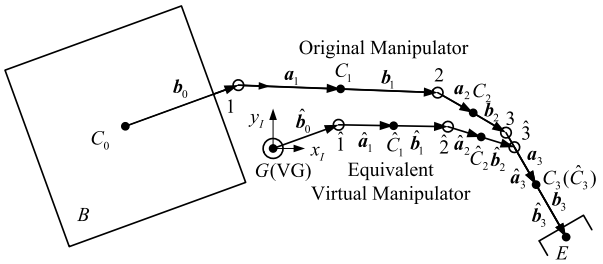

FIGURE 5. Equivalent VM of the 3-DOF free-floating space manipulator.

Readers can find the detailed kinematics modeling process in Appendix and [34].

B. RS FOR THE 3-DOF FREE-FLOATING SPACE MANIPULATOR

For the task that requires end-effector to track a predefined path to arrive at desired position/attitude, we select end-effector position/attitude as representation variables to construct RS. When considering some predefined constraints, the unreachable regions will appear in RS correspondingly. The constraints just produce some unreachable regions, but they will not influence the fundamental principle of the RS analytical method. Thus for convenience, we don't consider constraints in establishing RS for the 3-DOF free-floating space manipulator.

End-effector position/attitude are selected as representation variables, and corresponding GCRV is $\boldsymbol{\xi} = [x_e(\boldsymbol{\theta}, \boldsymbol{r}_0, \Psi_0), y_e(\boldsymbol{\theta}, \boldsymbol{r}_0, \Psi_0), \Psi_e(\boldsymbol{\theta}, \boldsymbol{r}_0, \Psi_0)]^{\mathrm{T}} \in \mathbf{R}^3$. Thus RS is in 3-dimensional rectangular-coordinate. End-effector positions are in x-axis and y-axis, and end-effector attitude is in z-axis. When the linear momentum of manipulator system is conservative, GCRV becomes $\boldsymbol{\xi} = [x_e(\boldsymbol{\theta}, \Psi_0), y_e(\boldsymbol{\theta}, \Psi_0), \Psi_e(\boldsymbol{\theta}, \Psi_0)]^{\mathrm{T}} \in \mathbf{R}^3$.

We construct FRS, CRS, MRS, GRS and PGRS for the 3-DOF free-floating space manipulator.

1) FRS

Assuming $\boldsymbol{r}_0 = \boldsymbol{r}_0^{\text{const}}$, $\Psi_0 = \Psi_0^{\text{const}}$, FRS can be expressed as

$$\begin{aligned}\boldsymbol{R}_{\text{FRS}} = \{&[x_e, y_e, \Psi_e] | x_e = B_x^{\text{const}} + l_1 c_{01} + l_2 c_{012} + l_3 c_{0123}, \\ &y_e = B_y^{\text{const}} + l_1 s_{01} + l_2 s_{012} + l_3 s_{0123}, \\ &\Psi_e = \Psi_0^{\text{const}} + \theta_1 + \theta_2 + \theta_3, \\ &\theta_i^{\min} \le \theta_i \le \theta_i^{\max}, i = 1, 2, 3\} \quad (29)\end{aligned}$$

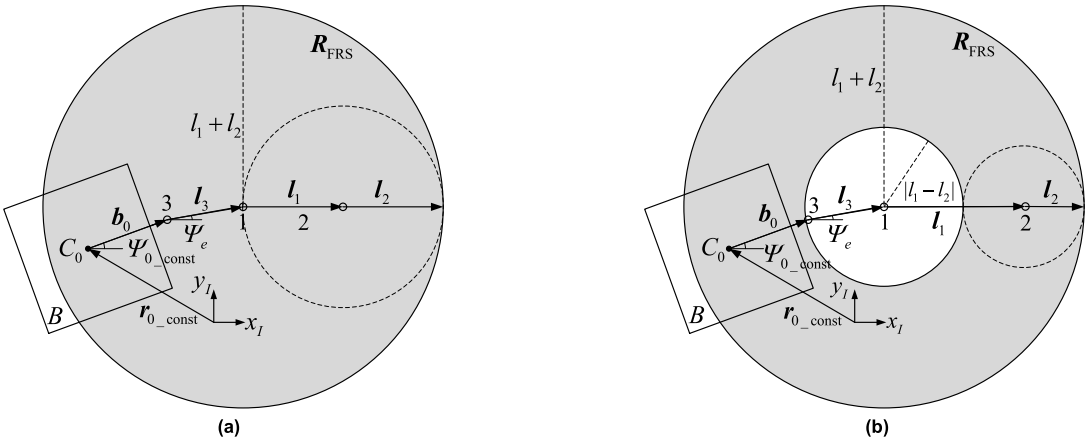

FIGURE 6. FRS section in Ψ_e. (a) $l_1 = l_2$. (b) $l_1 \neq l_2$.

where $B_x^{\text{const}} = r_{0x}^{\text{const}} + b_0 \cos\Psi_0^{\text{const}}$ and $B_y^{\text{const}} = r_{0y}^{\text{const}} + b_0 \sin\Psi_0^{\text{const}}$. When Ψ_e is determined, $l_3 c_{0123}$ and $l_3 s_{0123}$ are known, and we can obtain a FRS section in the determined Ψ_e. If $l_1 = l_2$, FRS section in the determined Ψ_e is a circle whose center is in $[B_x^{\text{const}} + l_3 c_{0123}, B_y^{\text{const}} + l_3 s_{0123}]$, and radius is $r = l_1 + l_2$. If $l_1 \neq l_2$, FRS section is an annulus whose center is in $[B_x^{\text{const}} + l_3 c_{0123}, B_y^{\text{const}} + l_3 s_{0123}]$, inner radius is $r_2 = |l_1 - l_2|$, and external radius is $r_1 = l_1 + l_2$. Fig.6 shows the FRS section.

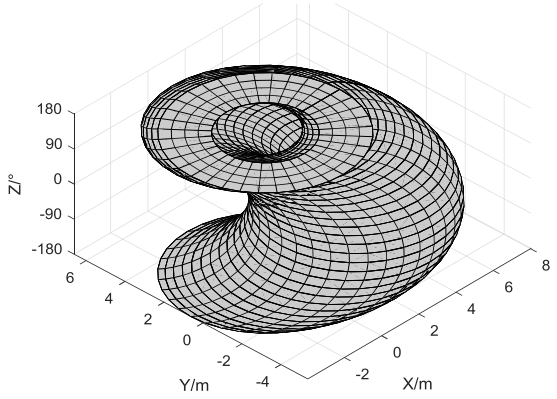

FIGURE 7. FRS ($R_0^{\text{const}} = [0.1, 0.1]^{\mathrm{T}} m$, $\Psi_0^{\text{const}} = 15°$ and $\hat{l}_1 \neq \hat{l}_2$).

Setting the link parameters as $b_0 = 2\text{m}$, $l_1 = 3\text{m}$, $l_2 = 1\text{m}$, $l_3 = 2\text{m}$, and assuming $\boldsymbol{r}_0^{\text{const}} = [0.1, 0.1]^{\mathrm{T}} m$ and $\Psi_0^{\text{const}} = 15°$. With Ψ_e varying in $[-180°, 180°]$, we can obtain FRS in Fig.7. From Fig.7, we can see that FRS is a hollow helix.

Projecting FRS onto *xy*-plane, we have Fig.8. The projection is a circle whose center is in red point [2.0319, 0.6176]m, and radius is $l_1 + l_2 + l_3 = 6\text{m}$. The projection of FRS eliminates end-effector attitude, and it is the fixed vehicle workspace of the manipulator [34].

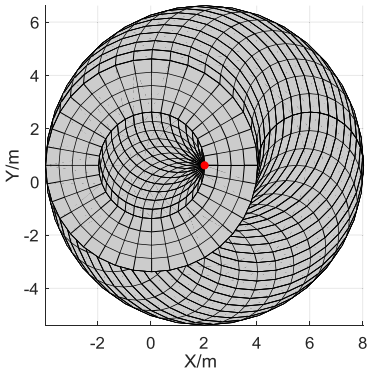

FIGURE 8. Projection of FRS onto *xy*-plane ($R_0^{\text{const}} = [0.1, 0.1]^{\mathrm{T}} m$, $\Psi_0^{\text{const}} = 15°$ and $\hat{l}_1 \neq \hat{l}_2$).

2) CRS

Assuming $\Psi_0 = \Psi_0^{\text{const}}$, CRS can be expressed as

$$\begin{aligned}\boldsymbol{R}_{\text{CRS}} = \{[x_e, y_e, \Psi_e] | x_e &= \hat{b}_0 \cos\Psi_0^{\text{const}} \\ &+ \hat{l}_1 c_{01} + \hat{l}_2 c_{012} + \hat{l}_3 c_{0123}, \\ y_e &= \hat{b}_0 \sin\Psi_0^{\text{const}} + \hat{l}_1 s_{01} + \hat{l}_2 s_{012} + \hat{l}_3 s_{0123}, \\ \Psi_e &= \Psi_0^{\text{const}} + \theta_1 + \theta_2 + \theta_3, \\ \theta_i^{\min} &\leq \theta_i \leq \theta_i^{\max}, i = 1, 2, 3\}\end{aligned} \tag{30}$$

If $\hat{l}_1 = \hat{l}_2$, CRS section in the determined Ψ_e is a circle whose center is in $[\hat{b}_0 \cos\Psi_0^{\text{const}} + \hat{l}_3 c_{0123}, \hat{b}_0 \sin\Psi_0^{\text{const}} + \hat{l}_3 s_{0123}]$, and radius is $\hat{r} = \hat{l}_1 + \hat{l}_2$. If $\hat{l}_1 \neq \hat{l}_2$, CRS section is an annulus whose center is in $[\hat{b}_0 \cos\Psi_0^{\text{const}} + \hat{l}_3 c_{0123}, \hat{b}_0 \sin\Psi_0^{\text{const}} + \hat{l}_3 s_{0123}]$, inner radius is $\hat{r}_2 = |\hat{l}_1 - \hat{l}_2|$, and external radius is $\hat{r}_1 = \hat{l}_1 + \hat{l}_2$. Fig.9 shows the CRS section.

Setting the link parameters of VM as $\hat{b}_0 = 20/11\text{m}$, $\hat{l}_1 = 123/44\text{m}$, $\hat{l}_2 = 127/132\text{m}$, $\hat{l}_3 = 65/33\text{m}$, and $\Psi_0^{\text{const}} = 15°$. With Ψ_e varying in $[-180°, 180°]$, we obtain CRS in Fig.10. CRS is a hollow helix.

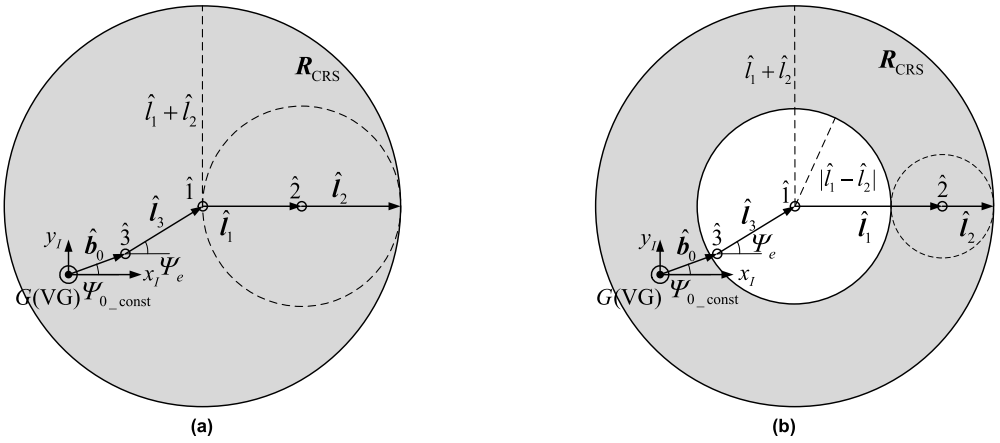

FIGURE 9. CRS section in Ψ_e. (a) $\hat{l}_1=\hat{l}_2$. (b) $\hat{l}_1\neq\hat{l}_2$.

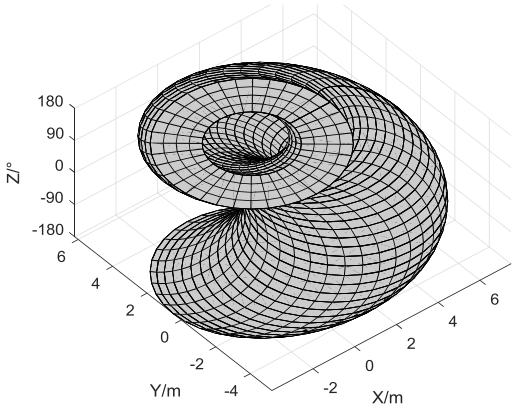

FIGURE 10. CRS ($\Psi_0^{\mathrm{const}}=15°$ and $\hat{l}_1\neq\hat{l}_2$).

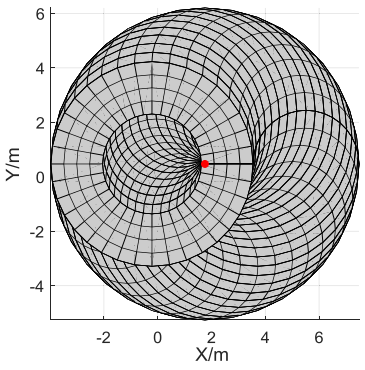

FIGURE 11. Projection of CRS onto *xy*-plane ($\Psi_0^{\mathrm{const}}=15°$ and $\hat{l}_1\neq\hat{l}_2$).

Projecting CRS onto *xy*-plane, we have Fig.11. The projection of CRS is a circle whose center is in red point [1.7562, 0.4709]m, and radius is $\hat{l}_1+\hat{l}_2+\hat{l}_3=63/11$m, and it is the attitude constrained workspace of the manipulator [34].

For the known end-effector position/attitude $[\mathbf{p}_e,\Psi_e]^{\mathrm{T}}$, its reachable range of base attitude can be expressed as

$$[\mathbf{p}_e,\Psi_e]^{\mathrm{T}}\Psi_0\in[[\mathbf{p}_e,\Psi_e]^{\mathrm{T}}\Psi_0^{\min},[\mathbf{p}_e,\Psi_e]^{\mathrm{T}}\Psi_0^{\max}] \tag{31}$$

3) MRS

MRS can be expressed as

$$\begin{aligned}\boldsymbol{R}_{\mathrm{MRS}}=\{&[x_e,y_e,\Psi_e]|x_e=\hat{b}_0\cos\Psi_0+\hat{l}_1c_{01}\\&+\hat{l}_2c_{012}+\hat{l}_3c_{0123},\\&y_e=\hat{b}_0\sin\Psi_0+\hat{l}_1s_{01}+\hat{l}_2s_{012}+\hat{l}_3s_{0123},\\&\Psi_e=\Psi_0+\theta_1+\theta_2+\theta_3,\\&\Psi_0^{\min}\le\Psi_0\le\Psi_0^{\max},\theta_i^{\min}\le\theta_i\le\theta_i^{\max},i=1,2,3\}\end{aligned} \tag{32}$$

For $[\Psi_0^{\min},\Psi_0^{\max}]=[-180°,180°]$, MRS is a union of CRS corresponding to base attitude traversing in $[-180°,180°]$

$$\boldsymbol{R}_{\mathrm{MRS}}=\bigcup_{\Psi_0\in[-180°,180°]}\boldsymbol{R}_{\mathrm{CRS}}^{\Psi_0} \tag{33}$$

Because CRS section in the determined Ψ_e is either a circle or an annulus, there are three cases for the union of CRS. If $\hat{b}_0>\hat{l}_1+\hat{l}_2$, MRS section in the determined Ψ_e is an annulus whose center is in $[\hat{l}_3c_{0123},\hat{l}_3s_{0123}]$, inner radius is $\hat{r}_2=\hat{b}_0-\hat{l}_1+\hat{l}_2$, and external radius is $\hat{r}_1=\hat{b}_0+\hat{l}_1+\hat{l}_2$. If $\hat{b}_0=\hat{l}_1+\hat{l}_2$, or $\hat{l}_1=\hat{l}_2$ and $\hat{b}_0\le\hat{l}_1+\hat{l}_2$, or $\hat{l}_1\neq\hat{l}_2$ and $|\hat{l}_1-\hat{l}_2|\le\hat{b}_0<\hat{l}_1+\hat{l}_2$, MRS section is a circle whose center is in $[\hat{l}_3c_{0123},\hat{l}_3s_{0123}]$, and radius is $\hat{r}=\hat{b}_0+\hat{l}_1+\hat{l}_2$. If $\hat{l}_1\neq\hat{l}_2$ and $0\le\hat{b}_0<|\hat{l}_1-\hat{l}_2|$, MRS section is an annulus whose center is in $[\hat{l}_3c_{0123},\hat{l}_3s_{0123}]$, inner radius is $\hat{r}_2=|\hat{l}_1-\hat{l}_2|-\hat{b}_0$, and external radius is $\hat{r}_1=\hat{b}_0+\hat{l}_1+\hat{l}_2$. Fig.12 shows the MRS section.

Where Ψ_{01}, Ψ_{02}, Ψ_{03}, Ψ_{04} represent different of base attitude, and $C_{\Psi_{01}}$, $C_{\Psi_{02}}$, $C_{\Psi_{03}}$, $C_{\Psi_{04}}$ are corresponding CRS circles. Setting $\hat{b}_0=24/11$m, $\hat{l}_1=56/33$m, $\hat{l}_2=56/33$m, $\hat{l}_3=65/33$m, so $\hat{b}_0=\hat{l}_1+\hat{l}_2$. With Ψ_e varying in $[-180°,180°]$, we have MRS in Fig.13. MRS is a helix.

Projecting MRS onto *xy*-plane, we have Fig.14. The projection is a circle whose center is in red point [0, 0], and radius is $\hat{b}_0+\hat{l}_1+\hat{l}_2+\hat{l}_3=83/11$m. It is the maximum reachable workspace of the manipulator [34].

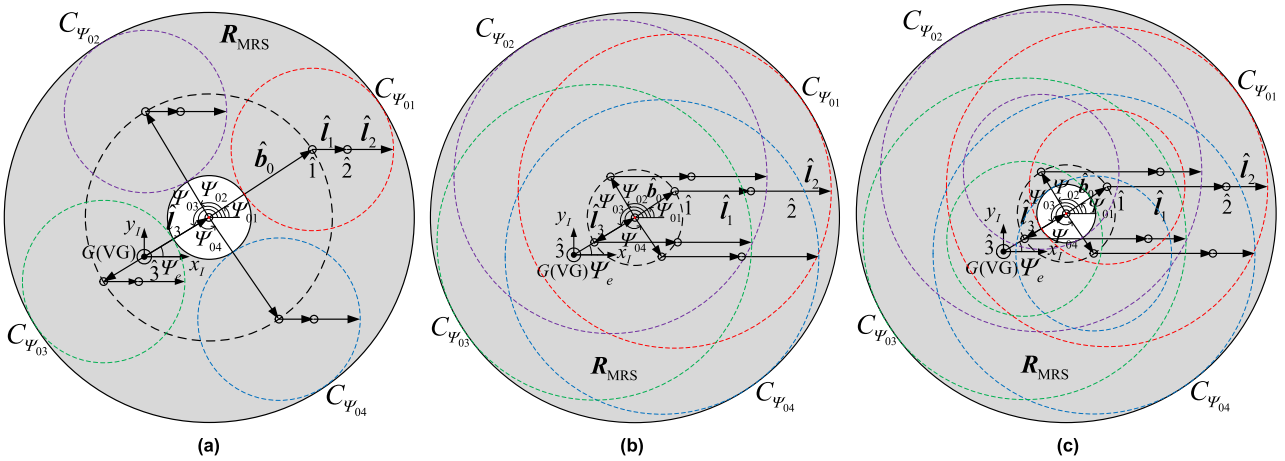

FIGURE 12. MRS section in Ψ_e. (a) $\hat{b}_0 > \hat{l}_1 + \hat{l}_2$. (b) $\hat{l}_1 = \hat{l}_2$ and $\hat{b}_0 \le \hat{l}_1 + \hat{l}_2$. (c) $\hat{l}_1 \ne \hat{l}_2$ and $0 \le \hat{b}_0 < |\hat{l}_1 - \hat{l}_2|$.

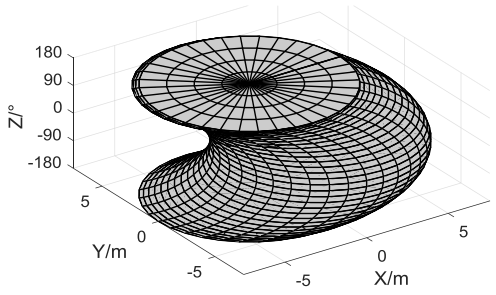

FIGURE 13. MRS ($\hat{l}_1 = \hat{l}_2$ and $\hat{b}_0 \le \hat{l}_1 + \hat{l}_2$).

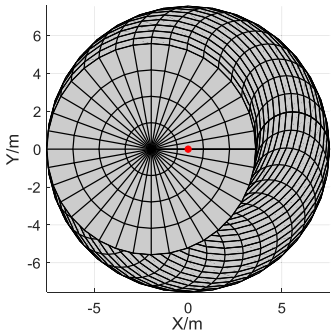

FIGURE 14. Projection of MRS onto *xy*-plane ($\hat{l}_1 = \hat{l}_2$ and $\hat{b}_0 \le \hat{l}_1 + \hat{l}_2$).

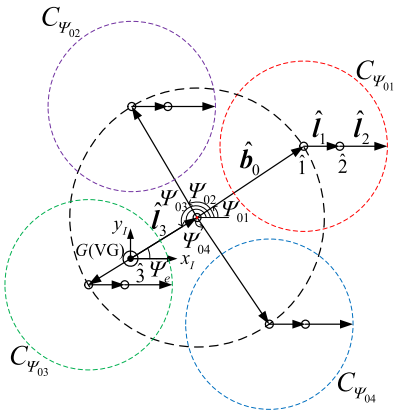

FIGURE 15. Intersection of all CRS sections in Ψ_e ($\hat{b}_0 \ge \hat{l}_1 + \hat{l}_2$).

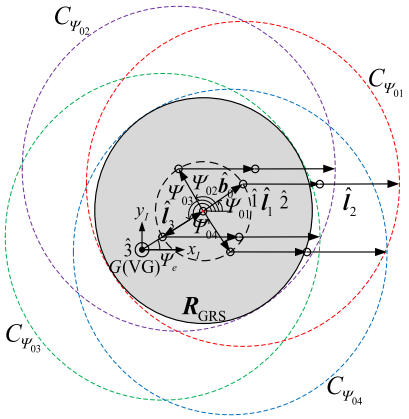

FIGURE 16. GRS section in Ψ_e ($\hat{l}_2 = \hat{l}_1$ and $0 \le \hat{b}_0 < \hat{l}_1 + \hat{l}_2$).

4) GRS

GRS is an intersection of all CRS corresponding to base attitudes traversing in $[-180°, 180°]$

$$\boldsymbol{R}_{\mathrm{GRS}} = \bigcap_{\Psi_0 \in [-180°, 180°]} \boldsymbol{R}_{\mathrm{CRS}}^{\Psi_0} \tag{34}$$

CRS section is either a circle or an annulus, so intersection of CRS has many cases.

Case A $\hat{b}_0 \ge \hat{l}_1 + \hat{l}_2$

Because $\hat{b}_0$ is very large, an intersection of all CRS is a null set, i.e. $\boldsymbol{R}_{\mathrm{GRS}} = \emptyset$. Meanwhile, the guaranteed workspace of the manipulator is also a null set [34]. An intersection of CRS sections is in Fig.15.

Case B $\hat{l}_2 = \hat{l}_1$ and $0 \le \hat{b}_0 < \hat{l}_1 + \hat{l}_2$.

In this case, CRS section is a circle, and GRS section is in Fig.16. It is a circle whose center is in $[\hat{l}_3 c_{0123}, \hat{l}_3 s_{0123}]$, and radius is $\hat{r} = \hat{l}_1 + \hat{l}_2 - \hat{b}_0$, and it inscribes all CRS sections.

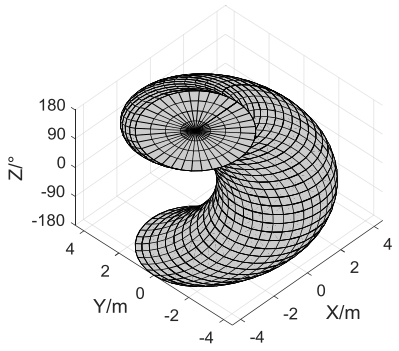

FIGURE 17. GRS ($\hat{l}_2 = \hat{l}_1$ and $0 \le \hat{b}_0 < \hat{l}_1 + \hat{l}_2$).

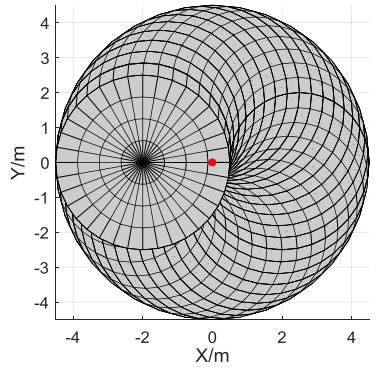

FIGURE 18. Projection of GRS onto *xy*-plane ($\hat{l}_2 = \hat{l}_1$ and $0 \le \hat{b}_0 < \hat{l}_1 + \hat{l}_2$).

Setting $\hat{b}_0 = 1.5\text{m}, \hat{l}_1 = 2\text{m}, \hat{l}_2 = 2\text{m}, \hat{l}_3 = 2\text{m}$. With end-effector attitude varying in $[-180°, 180°]$, GRS is in Fig.17, and it is a helix.

Projecting GRS onto *xy*-plane, we have Fig.18. The projection of GRS is a circle whose center is in red point [0, 0], and radius is $\hat{l}_1 + \hat{l}_2 + \hat{l}_3 - \hat{b}_0 = 4.5\text{m}$, and it is the guaranteed workspace of the manipulator [34].

If $\hat{l}_1 \neq \hat{l}_2$, CRS section is an annulus, and we have following cases.

Case C $\max(\hat{l}_1, \hat{l}_2) \le \hat{b}_0 < \hat{l}_1 + \hat{l}_2$

GRS section is in Fig.19. It is a circle whose center is in $[\hat{l}_3 c_{0123}, \hat{l}_3 s_{0123}]$, and radius is $\hat{r} = \hat{l}_1 + \hat{l}_2 - \hat{b}_0$, and it inscribes all the external circles of CRS annuluses.

Making $\hat{b}_0 = 2.5\text{m}, \hat{l}_1 = 2\text{m}, \hat{l}_2 = 1\text{m}, \hat{l}_3 = 2\text{m}$, GRS is in Fig.20, and it is a helix.

Projecting GRS onto *xy*-plane, we have Fig.21. The projection is an annulus whose center is in red point [0, 0], inner radius is $\hat{l}_3 + \hat{b}_0 - (\hat{l}_1 + \hat{l}_2) = 1.5\text{m}$, and external radius is $\hat{l}_1 + \hat{l}_2 + \hat{l}_3 - \hat{b}_0 = 2.5\text{m}$. But the guaranteed workspace now is a circle whose center is in [0, 0], and radius is 2.5m [34]. Thus the projection of GRS is a subset of the guaranteed workspace.

Case D $\min(\hat{l}_1, \hat{l}_2) < \frac{1}{2}\max(\hat{l}_1, \hat{l}_2)$ and $|\hat{l}_1 - \hat{l}_2| < \hat{b}_0 \le \max(\hat{l}_1, \hat{l}_2)$, or $\frac{1}{2}\max(\hat{l}_1, \hat{l}_2) \le \min(\hat{l}_1, \hat{l}_2) < \max(\hat{l}_1, \hat{l}_2)$ and $\min(\hat{l}_1, \hat{l}_2) < \hat{b}_0 \le \max(\hat{l}_1, \hat{l}_2)$.

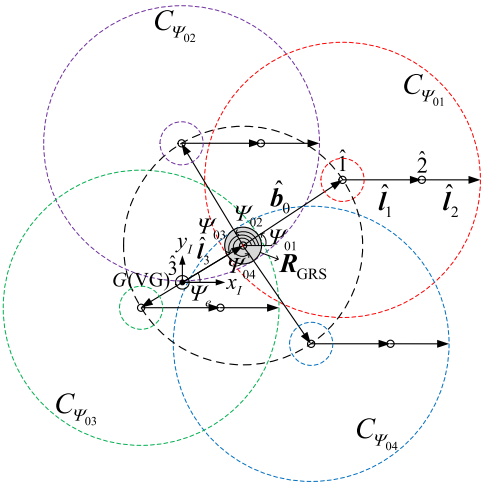

FIGURE 19. GRS section in Ψ_e ($\hat{l}_2 < \hat{l}_1$ and $\hat{l}_1 \le \hat{b}_0 < \hat{l}_1 + \hat{l}_2$).

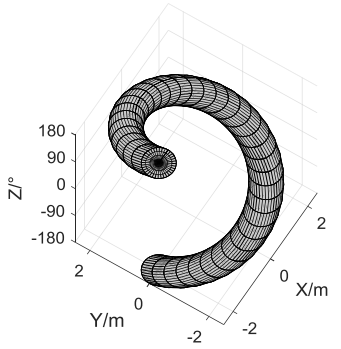

FIGURE 20. GRS ($\hat{l}_2 < \hat{l}_1$ and $\hat{l}_1 \le \hat{b}_0 < \hat{l}_1 + \hat{l}_2$).

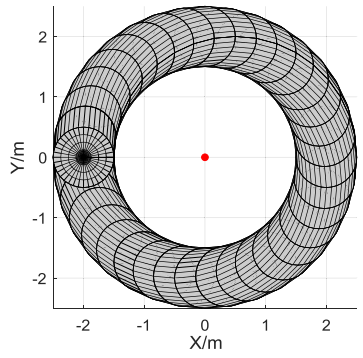

FIGURE 21. Projection of GRS onto *xy*-plane ($\hat{l}_2 < \hat{l}_1$ and $\hat{l}_1 \le \hat{b}_0 < \hat{l}_1 + \hat{l}_2$).

GRS section is in Fig.22. It is a circle whose center is in $[\hat{l}_3 c_{0123}, \hat{l}_3 s_{0123}]$, and radius is $\hat{r} = \hat{b}_0 - |\hat{l}_1 - \hat{l}_2|$, and it circumscribes the inner circles of CRS annulus.

Setting $\hat{b}_0 = 2.5\text{m}, \hat{l}_1 = 3\text{m}, \hat{l}_2 = 2\text{m}, \hat{l}_3 = 2\text{m}$, GRS is in Fig.23. It is a helix.

Projecting GRS onto *xy*-plane, we have Fig.24. The projection is an annulus whose center is in red point [0, 0], inner radius is $\hat{l}_3 - \hat{b}_0 + |\hat{l}_1 - \hat{l}_2| = 0.5\text{m}$, and external radius is

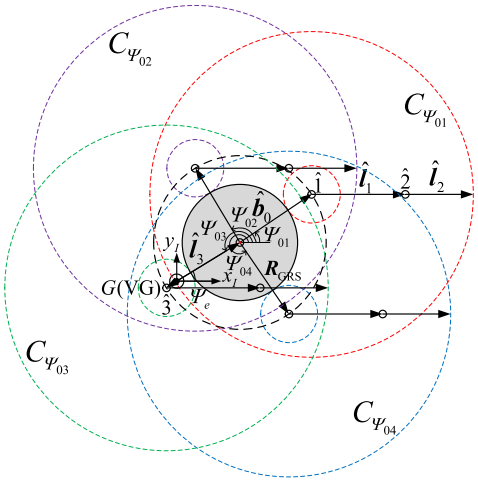

FIGURE 22. GRS section in Ψ_e ($\frac{\hat{l}_1}{2} \le \hat{l}_2 < \hat{l}_1$ and $\hat{l}_2 < \hat{b}_0 \le \hat{l}_1$).

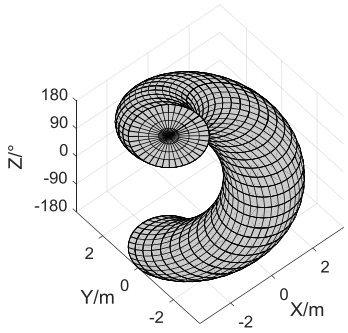

FIGURE 23. GRS ($\frac{\hat{l}_1}{2} \le \hat{l}_2 < \hat{l}_1$ and $\hat{l}_2 < \hat{b}_0 \le \hat{l}_1$).

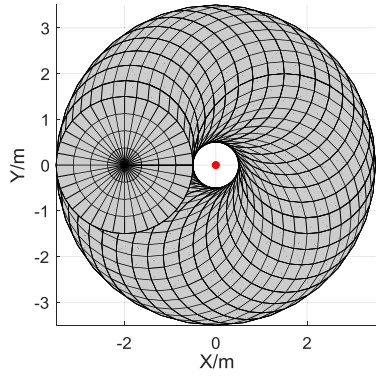

FIGURE 24. Projection of GRS onto *xy*-plane ($\frac{\hat{l}_1}{2} \le \hat{l}_2 < \hat{l}_1$ and $\hat{l}_2 < \hat{b}_0 \le \hat{l}_1$).

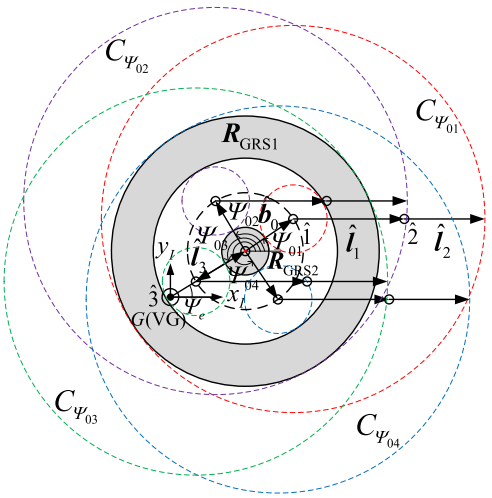

FIGURE 25. GRS section in Ψ_e ($\frac{\hat{l}_1}{2} < \hat{l}_2 < \hat{l}_1$ and $\hat{l}_1 - \hat{l}_2 < \hat{b}_0 \le \hat{l}_2$).

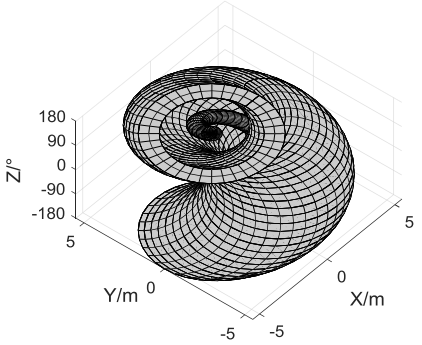

FIGURE 26. GRS ($\frac{\hat{l}_1}{2} < \hat{l}_2 < \hat{l}_1$ and $\hat{l}_1 - \hat{l}_2 < \hat{b}_0 \le \hat{l}_2$).

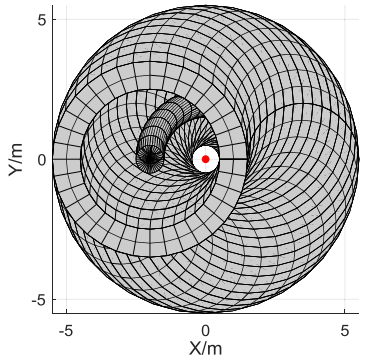

FIGURE 27. Projection of GRS onto *xy*-plane ($\frac{\hat{l}_1}{2} < \hat{l}_2 < \hat{l}_1$ and $\hat{l}_1 - \hat{l}_2 < \hat{b}_0 \le \hat{l}_2$).

$\hat{b}_0 - |\hat{l}_1 - \hat{l}_2| + \hat{l}_3 = 3.5$m. But the guaranteed workspace now is a circle whose center is in [0, 0] and radius is 3.5m [34]. Thus the projection of GRS is a subset of the guaranteed workspace.

Case E $\frac{1}{2}\max(\hat{l}_1, \hat{l}_2) < \min(\hat{l}_1, \hat{l}_2) < \max(\hat{l}_1, \hat{l}_2)$ and $|\hat{l}_1 - \hat{l}_2| < \hat{b}_0 \le \min(\hat{l}_1, \hat{l}_2)$

GRS section is in Fig.25. From Fig.25, we can see that GRS section is divided into two parts: $\boldsymbol{R}_{\mathrm{GRS1}}$ and $\boldsymbol{R}_{\mathrm{GRS2}}$. $\boldsymbol{R}_{\mathrm{GRS1}}$ is an annulus whose center is in $[\hat{l}_3 c_{0123}, \hat{l}_3 s_{0123}]$, inner radius is $\hat{r}_2 = \hat{b}_0 + |\hat{l}_1 - \hat{l}_2|$, and external radius is $\hat{r}_1 = \hat{l}_1 + \hat{l}_2 - \hat{b}_0$. $\boldsymbol{R}_{\mathrm{GRS2}}$ is a circle whose center is in $[\hat{l}_3 c_{0123}, \hat{l}_3 s_{0123}]$, and radius is $\hat{r} = \hat{b}_0 - |\hat{l}_1 - \hat{l}_2|$.

Setting $\hat{b}_0 = 1.5$m, $\hat{l}_1 = 3$m, $\hat{l}_2 = 2$m, $\hat{l}_3 = 2$m, GRS is in Fig.26. GRS is a nested helix.

Projecting GRS onto *xy*-plane, we have Fig.27. The projection is an annulus whose center is in red point [0, 0], and inner radius is $\hat{b}_0 + |\hat{l}_1 - \hat{l}_2| - \hat{l}_3 = 0.5$m, and external radius is $\hat{b}_0 - |\hat{l}_1 - \hat{l}_2| + \hat{l}_3 = 5.5$m. But the guaranteed workspace now is a circle whose center is in [0, 0] and radius is 5.5m [34]. Thus the projection of GRS is a subset of the guaranteed workspace.

Case F $\min(\hat{l}_1, \hat{l}_2) < \frac{1}{2}\max(\hat{l}_1, \hat{l}_2)$ and $0 \le \hat{b}_0 \le \min(\hat{l}_1, \hat{l}_2)$, or $\frac{1}{2}\max(\hat{l}_1, \hat{l}_2) \le \min(\hat{l}_1, \hat{l}_2) < \max(\hat{l}_1, \hat{l}_2)$ and $0 \le \hat{b}_0 \le |\hat{l}_1 - \hat{l}_2|$.

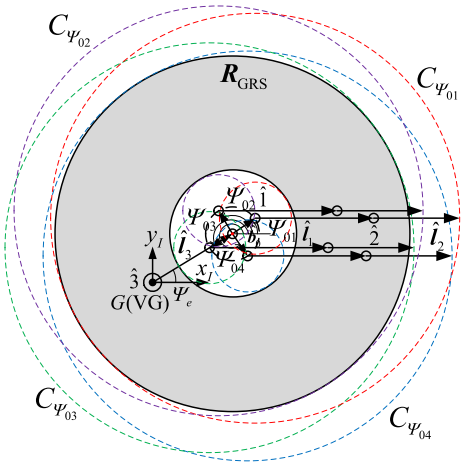

FIGURE 28. GRS section in Ψ_e ($\frac{\hat{l}_1}{2} \le \hat{l}_2 < \hat{l}_1$ and $0 < \hat{b}_0 \le \hat{l}_1 - \hat{l}_2$).

GRS section is in Fig.28. GRS section is an annulus whose center is in $[\hat{l}_3 c_{0123}, \hat{l}_3 s_{0123}]$, inner radius is $\hat{r}_2 = \hat{b}_0 + |\hat{l}_1 - \hat{l}_2|$, and external radius is $\hat{r}_1 = \hat{l}_1 + \hat{l}_2 - \hat{b}_0$.

Making $\hat{b}_0 = 0.5$m, $\hat{l}_1 = 3$m, $\hat{l}_2 = 2$m, $\hat{l}_3 = 2$m, GRS is in Fig.29, and it is a hollow helix.

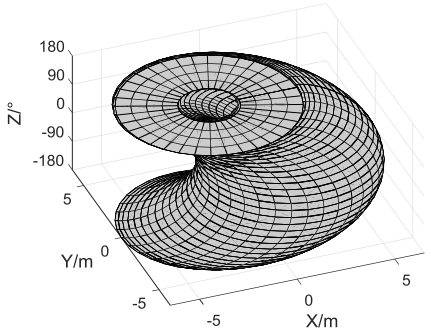

FIGURE 29. GRS ($\frac{\hat{l}_1}{2} \le \hat{l}_2 < \hat{l}_1$ and $0 < \hat{b}_0 \le \hat{l}_1 - \hat{l}_2$).

Projecting GRS onto *xy*-plane, we have Fig.30. The projection of GRS is a circle whose center is in red point [0, 0], and radius is $\hat{l}_1 + \hat{l}_2 + \hat{l}_3 - \hat{b}_0 = 6.5$m. It is the guaranteed workspace of the manipulator.

Case G $\min(\hat{l}_1, \hat{l}_2) < \frac{1}{2}\max(\hat{l}_1, \hat{l}_2)$ and $\min(\hat{l}_1, \hat{l}_2) \le \hat{b}_0 \le |\hat{l}_1 - \hat{l}_2|$.

The inner circles erase the intersection of external circles, so GRS is a null set, i.e. $\boldsymbol{R}_{\mathrm{GRS}} = \emptyset$. The intersection of

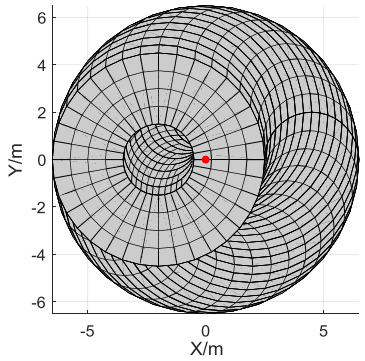

FIGURE 30. Projection of GRS onto *xy*-plane ($\frac{\hat{l}_1}{2} \le \hat{l}_2 < \hat{l}_1$ and $0 < \hat{b}_0 \le \hat{l}_1 - \hat{l}_2$).

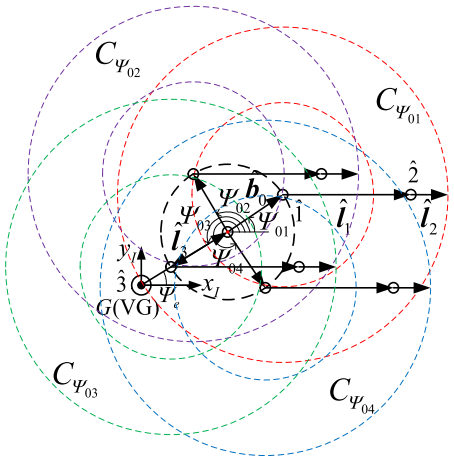

FIGURE 31. Intersection of all CRS sections in Ψ_e ($\min(\hat{l}_1, \hat{l}_2) < \frac{1}{2}\max(\hat{l}_1, \hat{l}_2)$ and $\min(\hat{l}_1, \hat{l}_2) \le \hat{b}_0 \le |\hat{l}_1 - \hat{l}_2|$).

CRS sections is shown in Fig.31. However, the guaranteed workspace now exists, and it is a circle whose center is in [0, 0] and radius is $\hat{r} = \hat{l}_1 + \hat{l}_2 + \hat{l}_3 - \hat{b}_0$ [34].

According to above analysis, the shape and existence of GRS entirely depend on the specific link parameters of VM. GRS is usually small or even empty(like case A, C, D, E, G), so path planning in GRS is prone to fail. Furthermore, in Case C, D, E, G, the projection of GRS is only a subset of the guaranteed workspace of the 3-DOF free-floating space manipulator. This is because compared to the guaranteed workspace, GRS additionally considers end-effector attitude, which causes the degradation of reachability of end-effector. Therefore path planning for tasks which requires reachability of end-effector position/attitude is more complicated.

5) PGRS

Because PGRS is an intersection of all CRS corresponding to base attitude traversing in the practical reachable range $[\Psi_0^{\mathrm{lower}}, \Psi_0^{\mathrm{upper}}]$, there are also many intersection cases. But the cases are similar to that of GRS, so we only give the case when $\hat{l}_2 = \hat{l}_1$ and $0 \le \hat{b}_0 < \hat{l}_1 + \hat{l}_2$. In this case, CRS section is a circle, and PGRS section is in Fig.32. Where $C_{\Psi_0^{\mathrm{lower}}}$ and

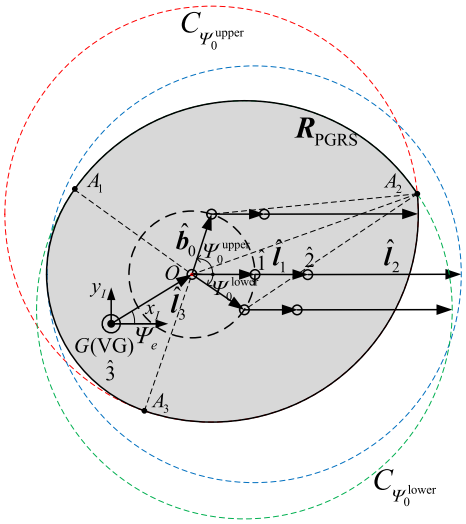

FIGURE 32. PGRS section in Ψ_e ($\hat{l}_2 \geq \hat{l}_1$ and $0 \leq \hat{b}_0 < \hat{l}_1 + \hat{l}_2$).

$C_{\Psi_0^{\text{upper}}}$ are the CRS sections corresponding to base attitude fixed in Ψ_0^{lower} and Ψ_0^{upper}, respectively. In Fig.32, PGRS section is a plane surrounded by (Part of boundary of $C_{\Psi_0^{\text{lower}}}$), (Part of boundary of $C_{\Psi_0^{\text{upper}}}$), and (The arc on the circle whose center is in $[\hat{l}_3 c_{0123}, \hat{l}_3 s_{0123}]$, radius is $\hat{r} = \hat{l}_1 + \hat{l}_2 - \hat{b}_0$, and central angle is $\Psi_0^{\text{upper}} - \Psi_0^{\text{lower}}$).

Setting $\hat{b}_0 = 1.5$m, $\hat{l}_1 = 2$m, $\hat{l}_2 = 2$m, $\hat{l}_3 = 2$m, and $[\Psi_0^{\text{lower}}, \Psi_0^{\text{upper}}] = [0, 90°]$, PGRS is in Fig.33. It is a helix.

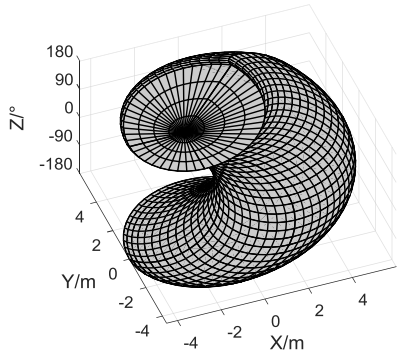

FIGURE 33. GRS ($\hat{l}_2 \geq \hat{l}_1$ and $0 \leq \hat{b}_0 < \hat{l}_1 + \hat{l}_2$).

Projecting PGRS onto xy-plane, we have Fig.34.

PGRS is bigger than GRS in Case B for the same VM, and the volume ratio between them is $V_{\boldsymbol{R}_{\text{PGRS}}}/V_{\boldsymbol{R}_{\text{GRS}}} = 1.5607$. Thus the path planning domain is expanded.

C. PATH TRACKING STRATEGY WITH NON-HOLONOMIC BEHAVIOR OF FREE-FLOATING MANIPULATORS

When the 3-DOF free-floating space manipulator tracks the path in PGRS, the base attitude should be limited in the practical reachable range. For this purpose, we design a path tracking strategy for the 3-DOF free-floating space manipulator based on non-holonomic motion planning method.

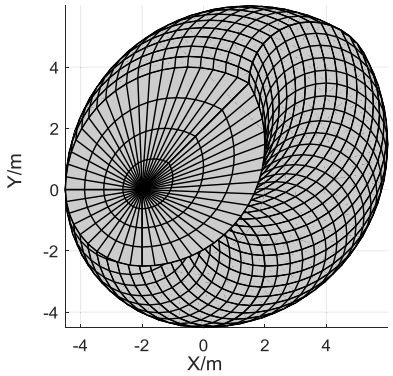

FIGURE 34. Projection of GRS onto xy-plane ($\hat{l}_2 \geq \hat{l}_1$ and $0 \leq \hat{b}_0 < \hat{l}_1 + \hat{l}_2$).

For the straight path whose the initial position/attitude are $[x_e^{\text{ini}}, y_e^{\text{ini}}, \Psi_e^{\text{ini}}]$ and the desired end-effector position/attitude are $[x_e^{\text{des}}, y_e^{\text{des}}, \Psi_e^{\text{des}}]$, the linear displacement and angular displacement are

$$d_{\text{linear}} = \sqrt{(x_e^{\text{des}} - x_e^{\text{ini}})^2 + (y_e^{\text{des}} - y_e^{\text{ini}})^2} \tag{35}$$

$$d_{\text{angular}} = \left|\Psi_e^{\text{ini}} - \Psi_e^{\text{des}}\right| \tag{36}$$

We interpolate the linear velocity $v(t)$ of end-effector with following quintic polynomial function

$$v(t) = a_0 + a_1 t + a_2 t^2 + a_3 t^3 + a_4 t^4 + a_5 t^5 \tag{37}$$

Angular velocity $\omega(t)$ of end-effector is interpolated as

$$\omega(t) = \frac{d_{\text{angular}}}{d_{\text{linear}}} v(t) \tag{38}$$

The units of d_{angular} and d_{linear} are ignored. Setting $t_0 = 0$ as the initial moment, t_e as the terminal moment, and Δt as interpolating interval, the total number of interpolating steps is $s = t_e / \Delta t$. The boundary conditions of the end-effector motion are as follow

$$\begin{cases} v(t_0) = a_0 = 0 \\ v(t_e) = a_0 + a_1 t_e + a_2 t_e^2 + a_3 t_e^3 + a_4 t_e^4 + a_5 t_e^5 = 0 \\ \dot{v}(t_0) = a_1 = 0 \\ \dot{v}(t_e) = a_1 + 2a_2 t_e + 3a_3 t_e^2 + 4a_4 t_e^3 + 5a_5 t_e^4 = 0 \\ \int_{t_0}^{t_e} v\mathrm{d}t = \sum_{i=1}^{s} [v(i\Delta t)\Delta t] = d_{\text{linear}} \end{cases} \tag{39}$$

Solving Eq.(39), we can express coefficients of the quintic polynomial function with a_5

$$\begin{cases} a_0 = 0 \\ a_1 = 0 \\ a_2 = \dfrac{-a_5 A_3 t_e^4 + 2a_5 A_4 t_e^3 - a_5 A_5 t_e^2 + t_e^2 B}{A_4 - 2A_3 t_e + A_2 t_e^2} \\ a_3 = \dfrac{a_5 A_2 t_e^4 - 3a_5 A_4 t_e^2 + 2a_5 A_5 t_e^5 - 2t_e B}{A_4 - 2A_3 t_e + A_2 t_e^2} \\ a_4 = \dfrac{-a_5 A_2 t_e^3 + 3a_5 A_3 t_e^2 - 2a_5 A_5 + B}{A_4 - 2A_3 t_e + A_2 t_e^2} \end{cases} \tag{40}$$

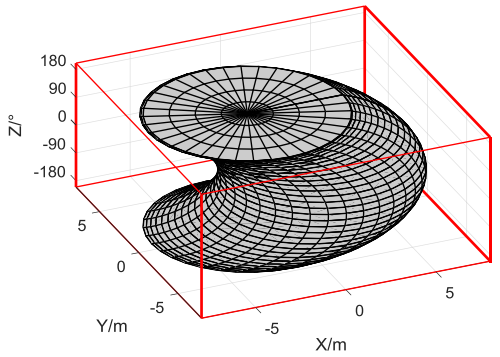

FIGURE 35. MRS.

where

$$\begin{cases} A_2 = \dfrac{s(s+1)(2s+1)}{6}\Delta t^2 \\ A_3 = \dfrac{s^2(s+1)^2}{4}\Delta t^3 \\ A_4 = \dfrac{s(s+1)(6s^3+9s^2+s-1)}{30}\Delta t^4 \\ A_5 = \dfrac{s^2(s+1)(2s^3+4s^2+s-1)}{12}\Delta t^5 \\ B = \dfrac{d_{\text{linear}}}{\Delta t} \end{cases}$$

If a_5 is determined, the interpolation will be achieved. Therefore, we only need to find the appropriate a_5 which can limit base attitude in practical reachable range. Thus the path tracking strategy can be expressed as the following mathematical model

$$\begin{aligned} &\text{find } a_5 \Rightarrow v(t, a_5) \\ &\text{s.t. } \Psi_0^{\text{lower}} \le \Psi_0(t) \le \Psi_0^{\text{upper}} \end{aligned} \tag{41}$$

Solving Eq.(41), the 3-DOF free-floating space manipulator can track path in PGRS to complete task successfully.

D. SIMULATION EXAMPLE OF PATH PLANNING FOR THE 3-DOF FREE-FLOATING SPACE MANIPULATOR

We verify the effectiveness of the RS analytical method and path planning strategy through a simulation experiment. The DH and dynamics parameters of the 3-DOF free-floating space manipulator are shown in Table 1 and Table 2.

TABLE 1. DH Parameters.

Joint i	$\alpha_{i-1}/(°)$	a_{i-1}/m	$\theta_i/(°)$	d_i/m
1	0	1.5m	θ_1	0
2	0	123/61m	θ_2	0
3	0	123/62m	θ_3	0
The length of the end-link is 2m.				

Thus $M = m_0 + m_1 + m_2 + m_3 = 630\text{kg}$, and the links parameters of VM are $\hat{b}_0 = 10/7\text{m}$, $\hat{a}_1 = 20/21\text{m}$, $\hat{b}_1 = 62/63\text{m}$, $\hat{a}_2 = 61/63\text{m}$, $\hat{b}_2 = 61/63\text{m}$, $\hat{a}_3 = 62/63\text{m}$, $\hat{b}_3 = 1\text{m}$, $\hat{l}_1 = \hat{a}_1 + \hat{b}_1 = 122/63\text{m}$, $\hat{l}_2 = \hat{a}_2 + \hat{b}_2 = 122/63\text{m}$, $\hat{l}_3 = \hat{a}_3 + \hat{b}_3 = 125/63\text{m}$. Assuming the initial configuration of the manipulator is $\boldsymbol{\theta}^{\text{ini}} = [30°, 90°, -30°]^{\text{T}}$, the initial base attitude is $\Psi_0^{\text{ini}} = 0°$(the corresponding initial end-effector position/attitude are $[x_e^{\text{ini}}, y_e^{\text{ini}}, \Psi_e^{\text{ini}}]^{\text{T}}$ =[2.1347m, 4.6294m, $90^{\circ}]^{\text{T}}$), the desired end-effector position/attitude are $[x_e^{\text{des}}, y_e^{\text{des}}, \Psi_e^{\text{des}}]^{\text{T}} = [0\text{m}, -4m, -90°]^{\text{T}}$, the theoretical reachable range base attitude is $[\Psi_0^{\min}, \Psi_0^{\max}] = [-180°, 180°]$, and the base attitude deflection limitation is $[{}^{\text{allow}}\Psi_0^{\min}, {}^{\text{allow}}\Psi_0^{\max}] = [-20°, 20°]$. The task requires end-effector move along a straight path to arrive at the desired position/attitude.

MRS of the 3-DOF free-floating space manipulator is shown in Fig.35.

To entirely cover RS, according to the scale of MRS, we utilize the cuboid(the red part in Fig.35) whose length is 16m, width is 16m and height is $(7 \times 180/\pi)°$ to rasterize RS. The cuboid surfaces intersect x-axis at $[-8, 0, 0]$m and $[8, 0, 0]$m, y-axis at $[0, -8, 0]$m and $[0, 8, 0]$m, and z-axis at $[0, 0, -3.5 \times 180/\pi]°$ and $[0, 0, 3.5 \times 180/\pi]°$, respectively. Discretizing the big cuboid into the uniformly distributing

TABLE 2. Dynamics Parameters.

Link i	${}^i\boldsymbol{a}_i$	${}^i\boldsymbol{b}_i$	m_i (kg)	I_i (kg·m)
Base 0	/	$[1.5\text{m}, 0]^{\text{T}}$	600	900
1	$[1.0\text{m}, 0]^{\text{T}}$	$[62/61\text{m}, 0]^{\text{T}}$	10	5/12
2	$[1.0\text{m}, 0]^{\text{T}}$	$[61/62\text{m}, 0]^{\text{T}}$	10	11.25
3	$[1.0\text{m}, 0]^{\text{T}}$	$[1.0\text{m}, 0]^{\text{T}}$	10	10/3

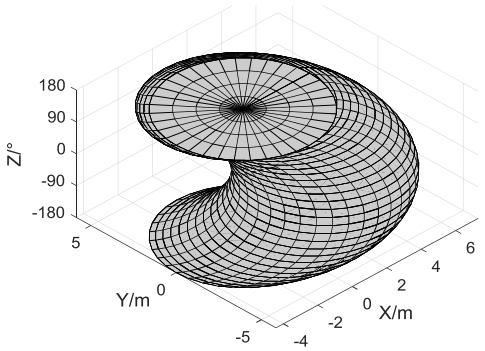

FIGURE 36. CRS ($\Psi_0 = 0°$).

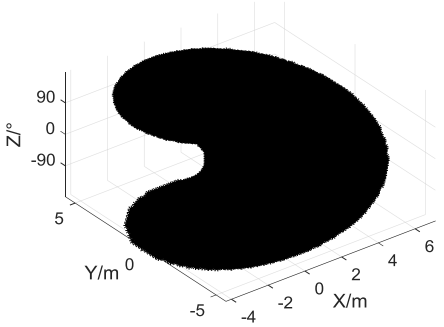

FIGURE 37. Rasterized CRS ($\Psi_0 = 0°$).

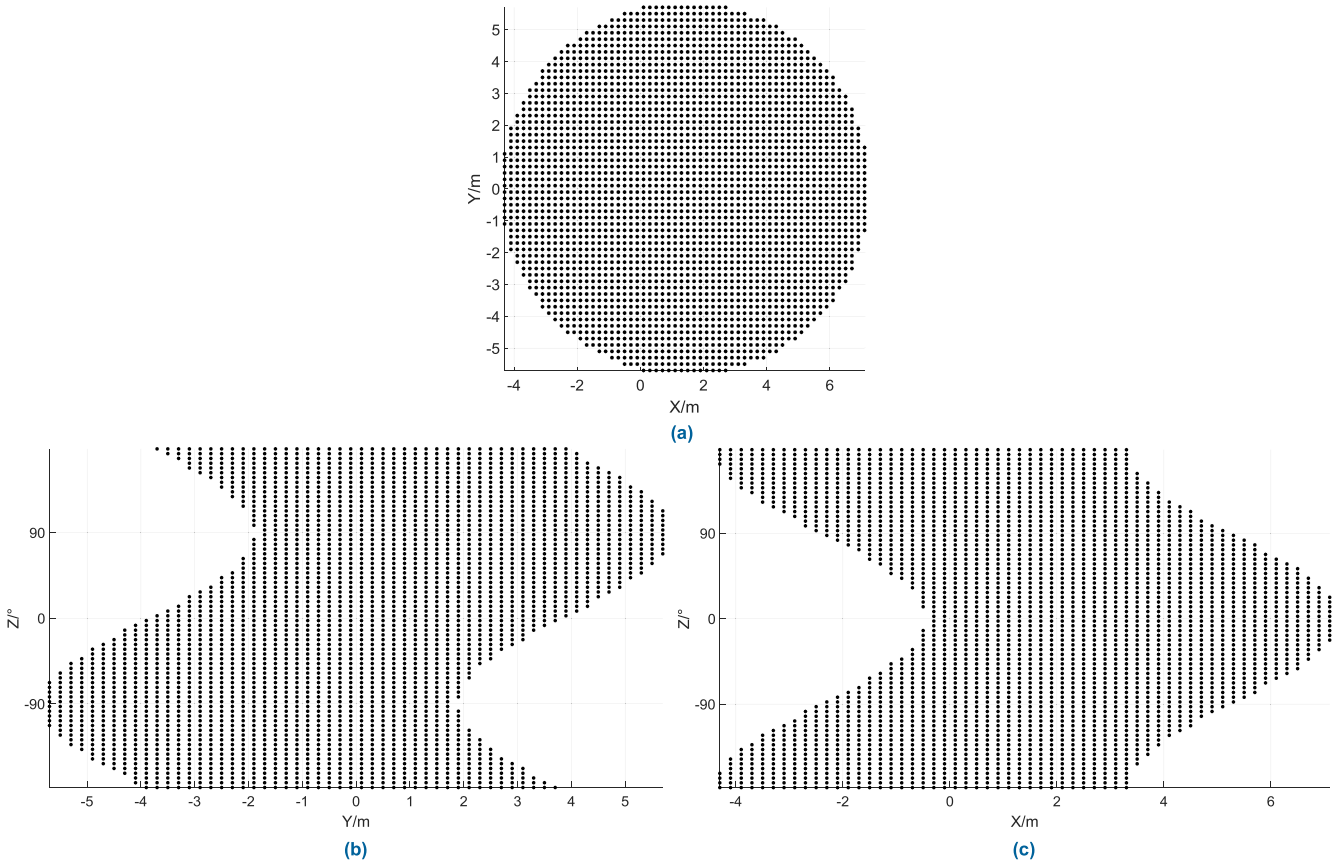

FIGURE 38. Projection of rasterized CRS ($\Psi_0 = 0°$). (a) Projection onto *xy*-plane. (b) Projection onto *yz*-plane. (c) Projection onto *xz*-plane.

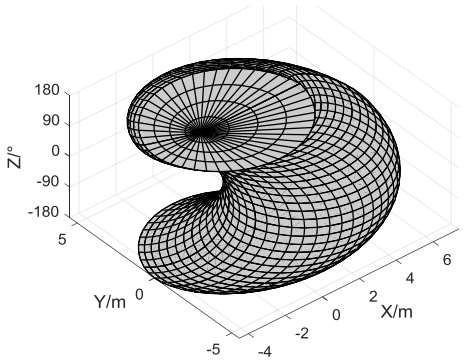

FIGURE 39. PGRS ($\Psi_0 \in [-20°, 20°]$).

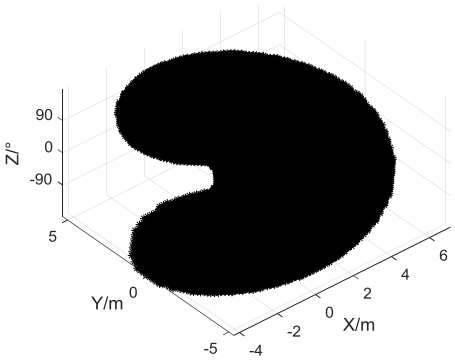

FIGURE 40. Rasterized PGRS ($\Psi_0 \in [-20°, 20°]$).

grids whose length is 0.2m, width is 0.2m, and height is $(0.0875 \times 180/\pi)°$, and finding the girds containing representation variables, CRS is rasterized. For example, for base attitude in $\Psi_0 = 0°$, CRS is in Fig.36. Utilizing center points of grids that contains representation variables to express the rasterized CRS, we have Fig.37. Projecting the rasterized CRS onto *xy*-plane, *yz*-plane and *xz*-plane, we have Fig.38. Every black point is the center point of the grid containing representation variables.

Judging the inclusion relations of the initial and desired position/attitude in all CRS, we can obtain the reachable base attitude ranges of the initial and desired position/attitude are $[{}^{\text{ini}}\Psi_0^{\min}, {}^{\text{ini}}\Psi_0^{\max}] = [-47°, 149°]$ and $[{}^{\text{des}}\Psi_0^{\min}, {}^{\text{des}}\Psi_0^{\max}] = [-180°, 180°]$, so the practical reachable range of base attitude is $\Psi_0 \in [\Psi_0^{\text{lower}}, \Psi_0^{\text{upper}}] = [-20°, 20°]$ from Eq.(20). PGRS and the rasterized PGRS are shown in Fig.41 and Fig.40, respectively. Projecting the rasterized PGRS onto *xy*-plane, *yz*-plane and *xz*-plane, we have Fig.41.

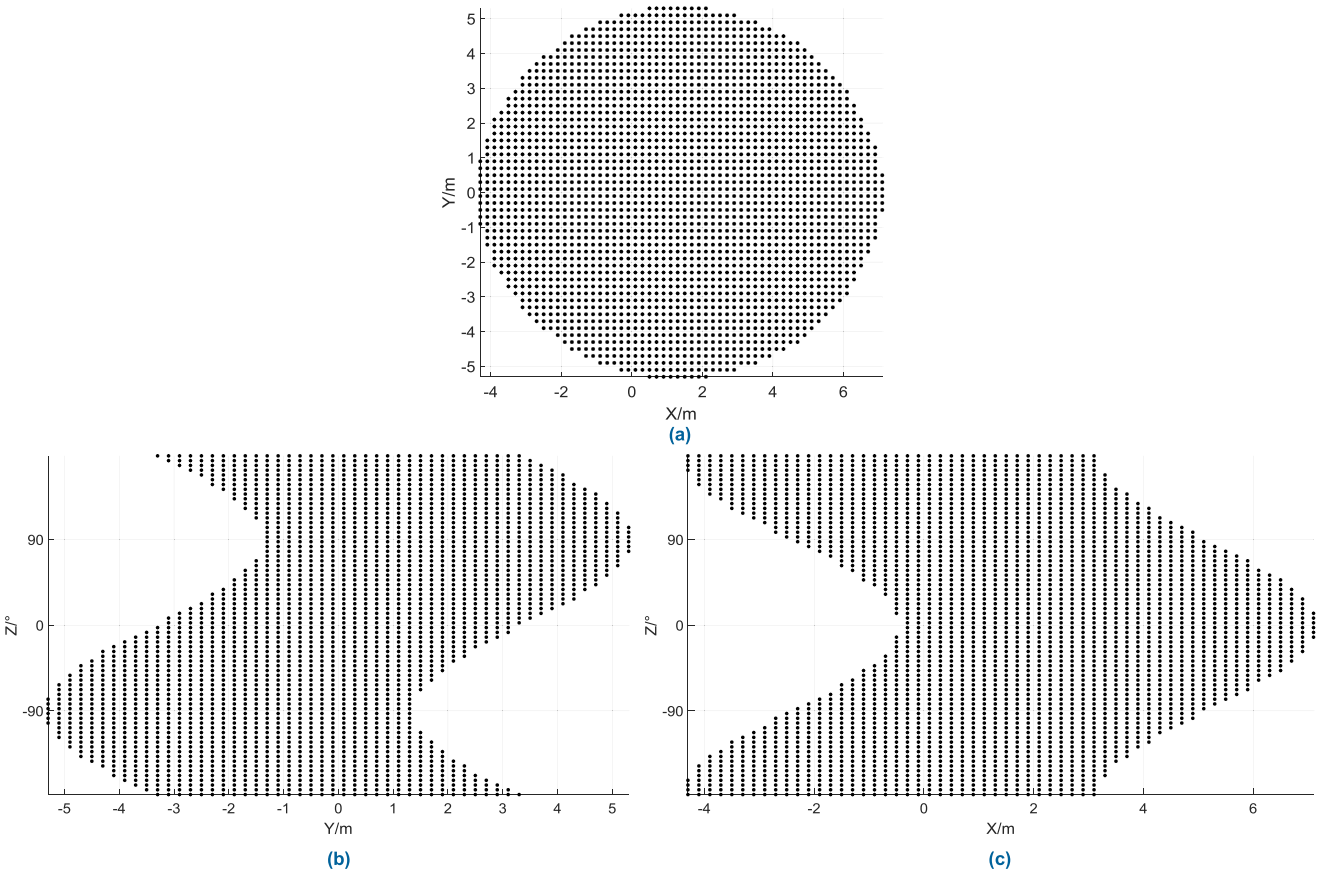

FIGURE 41. Projection of rasterized PGRS ($\Psi_0 \in [-20°, 20°]$). (a) Projection onto *xy*-plane. (b) Projection onto *yz*-plane. (c) Projection onto *xz*-plane.

TABLE 3. Middle Points of the Path.

Path Points	Coordinates
1(Initial Point)	$[2.1347\text{m}, 4.6294\text{m}, 90^\circ]^T$
2(Middle Point)	$[2.1\text{m}, 0.7\text{m}, -12.5363^\circ]^T$
3(Desired Point)	$[0\text{m}, -4\text{m}, -90^\circ]$

Because $[\Psi_0^{\text{lower}}, \Psi_0^{\text{upper}}] \subseteq [{}^{\text{ini}}\Psi_0^{\text{min}}, {}^{\text{ini}}\Psi_0^{\text{max}}]$ and $[\Psi_0^{\text{lower}}, \Psi_0^{\text{upper}}] \subseteq [{}^{\text{des}}\Psi_0^{\text{min}}, {}^{\text{des}}\Psi_0^{\text{max}}]$, PGRS absolutely contains the initial and desired position/attitude. Planning path in the rasterized PGRS through A* algorithm, we can obtain the path connecting the initial and desired points, so task is realizable. The endpoints of the path are in Table 3.

The time spent on searching path is 0.2135s, which means the path searching procedure is fast enough. The path consists of two segments, and all points in the path are reachable. The space manipulator tracks the first straight segment from the initial point to the middle point, then the manipulator further tracks the second straight segment from the middle point to the desired point, and task is finished. The obtained path is shown in Fig.42.

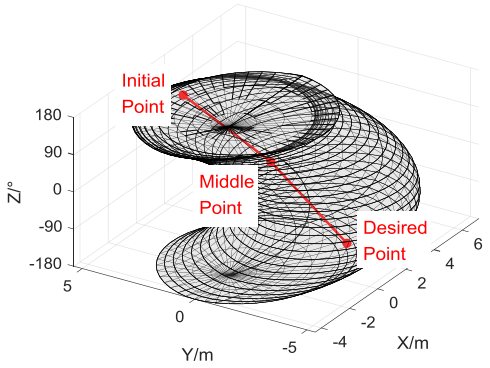

FIGURE 42. Path in PGRS.

When $a_5 = 0$, the manipulator can track the path to complete task and maintain base attitude in $[-20°, 20°]$. The planning parameters of two segments are in Table 4.

When the manipulator performs the task, the velocities of end-effector and joints, and the variation of base attitude are in Fig.43-Fig.45. It can be observed that the 3-DOF free-floating space manipulator preforms the task steadily, and maximum base attitude deflection doesn't exceed 3°.

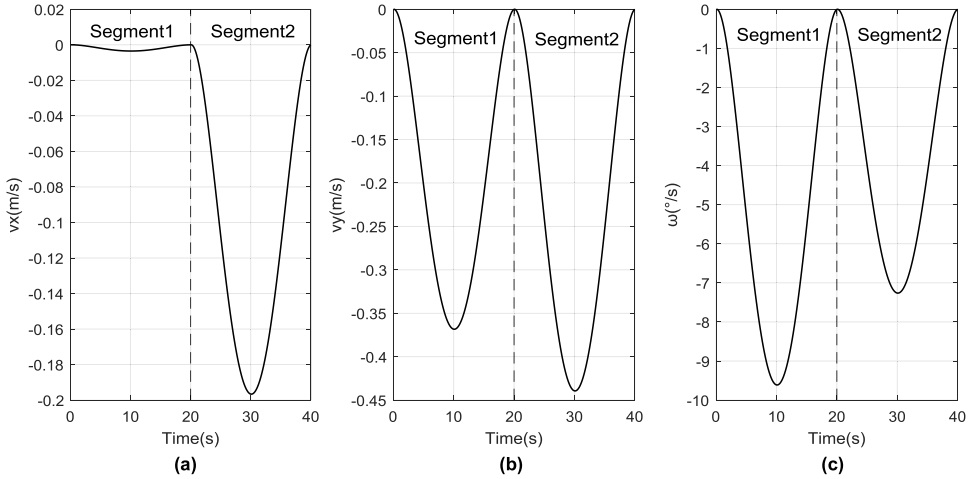

FIGURE 43. Velocity of End-effector. (a) Velocity in *x*-axis. (b) Velocity in *y*-axis. (c) Angular Velocity in *z*-axis.

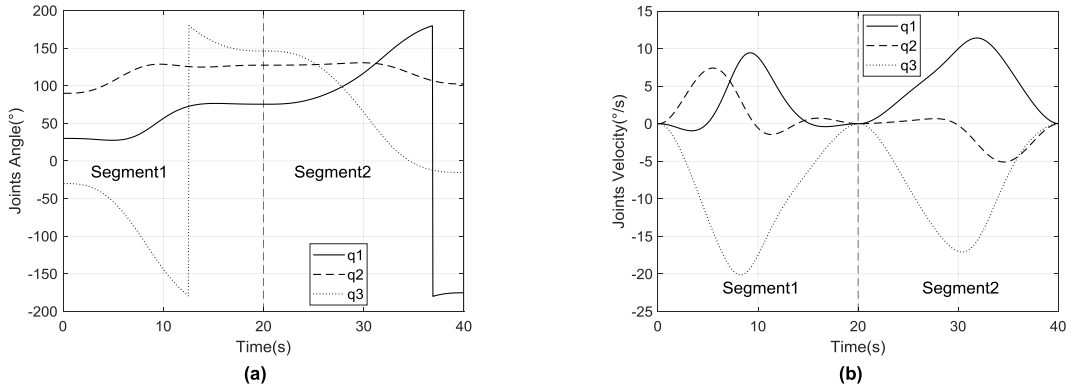

FIGURE 44. Joints motion. (a) Joints Angle. (b) Joints Velocity.

TABLE 4. Parameters of the Path.

Parameters	Segment 1	Segment 2
d_{linear}	3.9296m	5.1478m
d_{angular}	102.5363°	77.4637°
t_0	0s	0s
t_e	20s	20s
Δt	0.05s	0.05s
s	400	400
a_5	0	0
a_2	0.0147	0.0193
a_3	−0.0015	−0.0019
a_4	3.6840×10^{-5}	4.8140×10^{-5}

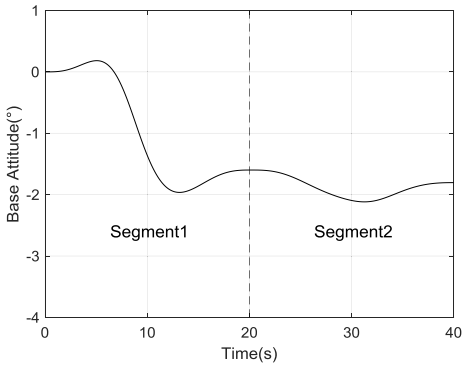

FIGURE 45. Variation of base attitude.

The motions of manipulator and base are shown in Fig.46. The blue part represents the motions of manipulator and base when tracking the first segment, and the red part represents the motions of manipulator and base when tracking the second segment. The black imaginary line represents the end-effector trajectory.

From the simulation results, aiming at the end-effector transposition task, task realizability evaluation and path planning for the 3-DOF free-floating space manipulator are accomplished in PGRS, and the manipulator can track the obtained path to complete task successfully.

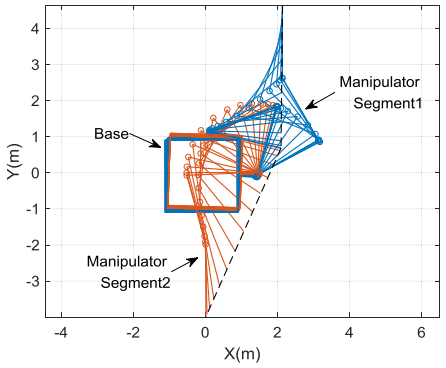

FIGURE 46. The motion of manipulator and base.

Therefore, effectiveness and practicability of the RS analytical method are verified.

V. CONCLUSION

We propose the RS analytical method for task realizability evaluation and path planning domain construction for free-floating space manipulators in this paper. The RS depends on the selection of representation variables. For free-floating space manipulators, the manipulator system variables which can accurately reflect the task attributes and base-coupled motion simultaneously are selected as representation variables to construct RS. We classify RS into FRS, CRS, MRS, GRS and PGRS according to different base control modes, and discuss the effects of different types of RS on task realizability evaluation and path planning. Then we know because appropriately considering the practical base attitude deflection limitation, only PGRS can be applied to evaluate task realizability and construct a path planning domain for free-floating space manipulators. When space manipulators track the path in PGRS, we maintain base attitude in the practical reachable range through the non-holonomic motion planning method. Taking the 3-DOF free-floating space manipulator as example, we select end-effector position/attitude as representation variables to visually show RS. A simulation experiment for path planning of the 3-DOF free-floating space manipulator is designed. Task realizability and path planning are accomplished in PGRS, and the manipulator can track the obtained path to complete task successfully. Therefore, effectiveness and practicability of the RS analytical method are verified.

The research possesses following traits:

1 The effects of base-coupled motion are integrated into the RS analytical method for the first time, and we provide a general path planning method for free-floating space manipulators theoretically.

2 According to different base control modes, we construct 5 types of RS. Different types of RS have different effects on task realizability evaluation and path planning domain construction of free-floating space manipulator. Among them, CRS illustrates the variation of base attitude mainly influences task realizability and acts on path planning, so we should consider the control of coupled motion of base attitude when manipulators work. Because appropriately considering the practical base attitude deflection limitation, PGRS can be applied to task realizability evaluation and path planning domain construction for free-floating space manipulators.

3 The RS analytical method is general for various manipulators(such as underwater robot, mobile robot and multiple cooperative robots) and tasks. In practical applications, we should select representation variables which can reflect task and manipulator attributes to construct RS.

In future work, we are going to apply the RS analytical method to some specific typical space tasks for space manipulators, such as load carrying task, module assembling task, target capturing task, etc., to further clarify the practicability and universality of the RS analytical method.

APPENDIX

We give the detailed kinematics modeling process of the n-DOF free-floating space manipulator in Appendix.

The positions of C_i and end-effector are

$$\boldsymbol{r}_i = \boldsymbol{r}_0 + \boldsymbol{b}_0 + \sum_{k=1}^{i-1} \boldsymbol{l}_k + \boldsymbol{a}_i \tag{42}$$

$$\boldsymbol{p}_e = \boldsymbol{R}_0 + \boldsymbol{b}_0 + \sum_{k=1}^{n} \boldsymbol{l}_k \tag{43}$$

Calculating derivatives of Eq.(42)-(43), we can obtain linear velocities of C_i and end-effector

$$\boldsymbol{v}_i = \dot{\boldsymbol{r}}_i = \boldsymbol{v}_0 + \boldsymbol{\omega}_0 \times (\boldsymbol{R}_i - \boldsymbol{r}_0) + \sum_{k=1}^{i} \left[\boldsymbol{k}_k \times (\boldsymbol{R}_i - \boldsymbol{p}_k)\right] \dot{\theta}_k \tag{44}$$

$$\boldsymbol{v}_e = \dot{\boldsymbol{p}}_e = \boldsymbol{v}_0 + \boldsymbol{\omega}_0 \times (\boldsymbol{p}_e - \boldsymbol{r}_0) + \sum_{k=1}^{n} \left[\boldsymbol{k}_k \times (\boldsymbol{p}_e - \boldsymbol{p}_k)\right] \dot{\theta}_k \tag{45}$$

where $\boldsymbol{v}_0$ is the linear velocity of base centroid, and $\boldsymbol{\omega}_0$ is the angular velocity of base. $\boldsymbol{k}_k$ is the unit vector of the k-th joint axis. Making $\boldsymbol{r}_{0i} = \boldsymbol{r}_i - \boldsymbol{r}_0$ and $\boldsymbol{p}_{0e} = \boldsymbol{p}_e - \boldsymbol{r}_0$, and expressing the cross product as the antisymmetric matrix multiplication

$$\begin{aligned}
\boldsymbol{\omega}_0 \times (\boldsymbol{r}_i - \boldsymbol{r}_0) &= \boldsymbol{\omega}_0 \times \boldsymbol{r}_{0i} \\
&= -\begin{bmatrix} 0 & -r_{0iz} & r_{0iy} \\ r_{0iz} & 0 & -r_{0ix} \\ -r_{0iy} & r_{0ix} & 0 \end{bmatrix} \boldsymbol{\omega}_0 = -\boldsymbol{r}_{0i}^{\times} \boldsymbol{\omega}_0 \\
\boldsymbol{\omega}_0 \times (\boldsymbol{p}_e - \boldsymbol{r}_0) &= \boldsymbol{\omega}_0 \times \boldsymbol{p}_{0e} \\
&= -\begin{bmatrix} 0 & -p_{0ez} & p_{0ey} \\ p_{0ez} & 0 & -p_{0ex} \\ -p_{0ey} & p_{0ex} & 0 \end{bmatrix} \boldsymbol{\omega}_0 = -\boldsymbol{p}_{0e}^{\times} \boldsymbol{\omega}_0
\end{aligned} \tag{46}$$

The angular velocities of the i-th link and end-effector are

$$\boldsymbol{\omega}_i = \boldsymbol{\omega}_0 + \sum_{k=1}^{i} \boldsymbol{k}_k \dot{\theta}_k \tag{47}$$

$$\boldsymbol{\omega}_e = \boldsymbol{\omega}_0 + \sum_{k=1}^{n} \boldsymbol{k}_k \dot{\theta}_k \tag{48}$$

Expressing Eq.(45) and Eq.(48) as the matrix from, we have

$$\begin{aligned}\begin{bmatrix} \boldsymbol{v}_e \\ \boldsymbol{\omega}_e \end{bmatrix} &= \begin{bmatrix} \boldsymbol{E} & -\boldsymbol{p}_{0e}^{\times} \\ \boldsymbol{O} & \boldsymbol{E} \end{bmatrix} \begin{bmatrix} \boldsymbol{v}_0 \\ \boldsymbol{\omega}_0 \end{bmatrix} \\ &\quad + \begin{bmatrix} \boldsymbol{k}_1 \times (\boldsymbol{p}_e - \boldsymbol{p}_1) & \cdots & \boldsymbol{k}_n \times (\boldsymbol{p}_e - \boldsymbol{p}_n) \\ \boldsymbol{k}_1 & \cdots & \boldsymbol{k}_n \end{bmatrix} \dot{\boldsymbol{\theta}} \\ &= \boldsymbol{J}_b \begin{bmatrix} \boldsymbol{v}_0 \\ \boldsymbol{\omega}_0 \end{bmatrix} + \boldsymbol{J}_m \dot{\boldsymbol{\theta}} \end{aligned} \tag{49}$$

where $\boldsymbol{E} \in \mathbf{R}^{3\times3}$ is a unit matrix, $\boldsymbol{O} \in \mathbf{R}^{3\times3}$ is a zero matrix. $\boldsymbol{J}_b \in \mathbf{R}^{6\times6}$ is the Jacobian matrix of base, and $\boldsymbol{J}_m \in \mathbf{R}^{6\times n}$ is the Jacobian matrix of manipulator. The linear momentum $\boldsymbol{P}$ and angular momentum $\boldsymbol{L}$ of overall system are

$$\boldsymbol{P} = \sum_{i=0}^{n} m_i \dot{\boldsymbol{r}}_i = \begin{bmatrix} M\boldsymbol{E} & -M\boldsymbol{r}_0^{\times \mathrm{T}} \end{bmatrix} \begin{bmatrix} \boldsymbol{v}_0 \\ \boldsymbol{\omega}_0 \end{bmatrix} + \boldsymbol{J}_{Tw} \dot{\boldsymbol{\theta}} \tag{50}$$

$$\boldsymbol{L} = \sum_{i=0}^{n} (\boldsymbol{I}_i \boldsymbol{\omega}_i + \boldsymbol{r}_i \times m_i \dot{\boldsymbol{r}}_i) = \begin{bmatrix} \boldsymbol{O} & \boldsymbol{I}_{\omega} \end{bmatrix} \begin{bmatrix} \boldsymbol{v}_0 \\ \boldsymbol{\omega}_0 \end{bmatrix} + \boldsymbol{I}_{\theta} \dot{\boldsymbol{\theta}} \tag{51}$$

where

$$\begin{aligned} \boldsymbol{J}_{Tw} &= \sum_{i=1}^{n} (m_i \boldsymbol{J}_{Ti}) \in \mathbf{R}^{3\times n} \\ \boldsymbol{I}_{\omega} &= \boldsymbol{I}_0 + \sum_{i=1}^{n} (\boldsymbol{I}_i + m_i \boldsymbol{r}_i^{\times} \boldsymbol{r}_{0i}^{\times \mathrm{T}}) \in \mathbf{R}^{3\times n} \\ \boldsymbol{I}_{\theta} &= \sum_{i=1}^{n} (\boldsymbol{I}_i \boldsymbol{J}_{Ri} + m_i \boldsymbol{r}_i^{\times} \boldsymbol{J}_{Ti}) \in \mathbf{R}^{3\times n} \\ \boldsymbol{J}_{Ti} &= [\boldsymbol{k}_1 \times (\boldsymbol{r}_i - \boldsymbol{p}_1), \cdots, \boldsymbol{k}_i \times (\boldsymbol{r}_i - \boldsymbol{p}_i), \boldsymbol{0}, \cdots, \boldsymbol{0}] \in \mathbf{R}^{3\times n} \\ \boldsymbol{J}_{Ri} &= [\boldsymbol{k}_1, \cdots, \boldsymbol{k}_i, \boldsymbol{0}, \cdots, \boldsymbol{0}] \in \mathbf{R}^{3\times n} \end{aligned}$$

For free-floating space manipulators, the system momentums are always conservative. Assuming the initial momentums of the whole system are zero, i.e. $\boldsymbol{P} = \boldsymbol{0}$ and $\boldsymbol{L} = \boldsymbol{0}$. From Eq.(50)-(51), we have

$$\begin{aligned}\begin{bmatrix} M\boldsymbol{E} & -M\boldsymbol{r}_0^{\times T} \\ \boldsymbol{O} & \boldsymbol{I}_{\omega} \end{bmatrix} \begin{bmatrix} \boldsymbol{v}_0 \\ \boldsymbol{\omega}_0 \end{bmatrix} + \begin{bmatrix} \boldsymbol{J}_{Tw} \\ \boldsymbol{I}_{\theta} \end{bmatrix} \dot{\theta} &= \boldsymbol{H}_b \begin{bmatrix} \boldsymbol{v}_0 \\ \boldsymbol{\omega}_0 \end{bmatrix} \\ &\quad + \boldsymbol{H}_{bm} \dot{\boldsymbol{\theta}} = \boldsymbol{0} \end{aligned} \tag{52}$$

So

$$\begin{bmatrix} \boldsymbol{v}_0 \\ \boldsymbol{\omega}_0 \end{bmatrix} = -\boldsymbol{H}_b^{-1} \boldsymbol{H}_{bm} \dot{\boldsymbol{\theta}} = \boldsymbol{J}_{bm} \dot{\boldsymbol{\theta}} \tag{53}$$

Eq.(53) illustrates coupled motions relationship between manipulator and base. Substituting Eq.(53) into Eq.(49), we have

$$\begin{bmatrix} \boldsymbol{v}_e \\ \boldsymbol{\omega}_e \end{bmatrix} = (\boldsymbol{J}_m + \boldsymbol{J}_b \boldsymbol{J}_{bm}) \dot{\boldsymbol{\theta}} = \boldsymbol{J}_g \dot{\boldsymbol{\theta}} \tag{54}$$

where $\mathbf{J}_g$ is the generalized Jacobian matrix. From Eq.(54), the inverse kinematics equation is

$$\dot{\boldsymbol{\theta}} = \boldsymbol{J}_g^{\dagger} \begin{bmatrix} \boldsymbol{v}_e \\ \boldsymbol{\omega}_e \end{bmatrix} \tag{55}$$

When $\mathrm{rank}(\boldsymbol{J}_g) < 6$, space manipulators are in singularity state, which means its end-effector can't move in some directions. Because $\boldsymbol{J}_g$ is related to the kinematics and dynamics parameters simultaneously, the singularity of space manipulator is called "Dynamic Singularity"[35].

The momentum of free-floating space manipulator system is conservative, and the linear momentum is always integrable. In time t, we have

$$\int_0^t \boldsymbol{P} \mathrm{d}t = \int_0^t \sum_{i=0}^{n} m_i \dot{\boldsymbol{r}}_i \mathrm{d}t = \sum_{i=0}^{n} m_i \boldsymbol{r}_i(t) - \sum_{i=0}^{n} m_i \boldsymbol{r}_i(0) = \boldsymbol{0} \tag{56}$$

According to $\boldsymbol{r}_g = \sum_{i=0}^{n} m_i \boldsymbol{r}_i \Big/ M$, we have $\sum_{i=0}^{n} m_i \boldsymbol{r}_i(t) - \sum_{i=0}^{n} m_i \boldsymbol{r}_i(0) = M\boldsymbol{r}_g(t) - M\boldsymbol{r}_g(0) = \boldsymbol{0}$, i.e. $\boldsymbol{r}_g(t) - \boldsymbol{r}_g(0) = \boldsymbol{0}$, which means the position of C_G is fixed when space manipulators perform tasks. Because $\sum_I$ is built in C_G, i.e. $\boldsymbol{r}_g(t) \equiv \boldsymbol{0}$, so we have

$$\sum_{i=0}^{n} m_i \boldsymbol{r}_i(t) = \boldsymbol{0} \tag{57}$$

Substituting Eq.(42) into Eq.(57), we obtain

$$\begin{aligned} \boldsymbol{r}_0 &= -\frac{m_1}{M}(\boldsymbol{b}_0 + \boldsymbol{a}_1) - \frac{m_2}{M}(\boldsymbol{b}_0 + \boldsymbol{l}_1 + \boldsymbol{a}_2) - \cdots \\ &\quad - \frac{m_n}{M}(\boldsymbol{b}_0 + \sum_{k=1}^{n-1} \boldsymbol{l}_k + \boldsymbol{a}_n) \\ &= -\sum_{q=1}^{n} \left[\frac{m_q}{M} \left(\boldsymbol{b}_0 + \boldsymbol{a}_q + \sum_{k=1}^{q-1} \boldsymbol{l}_k \right) \right] \end{aligned} \tag{58}$$

Substituting Eq.(58) into Eq.(43), we have

$$\boldsymbol{p}_e = -\sum_{q=1}^{n} \left[\frac{m_q}{M} \left(\boldsymbol{b}_0 + \boldsymbol{a}_q + \sum_{k=1}^{q-1} \boldsymbol{l}_k \right) \right] + \boldsymbol{b}_0 + \sum_{p=1}^{n} \boldsymbol{l}_p \tag{59}$$

From Eq.(59), $\boldsymbol{r}_0$ in $\boldsymbol{p}_e$ is eliminated. Substituting $\boldsymbol{l}_k = \boldsymbol{a}_k + \boldsymbol{b}_k$ into Eq.(59), we have Eq.(1).

REFERENCES

[1] J. W. McBarron, II, "Past, present, and future: The U.S. EVA program," *Acta Astronautica*, vol. 32, no. 1, pp. 5–14, Jan. 1994.
[2] D. Meng, Y. She, W. Xu, W. Lu, and B. Liang, "Dynamic modeling and vibration characteristics analysis of flexible-link and flexible-joint space manipulator," *Multibody Syst. Dyn.*, vol. 43, no. 4, pp. 321–347, Aug. 2018.
[3] X. Chen and S. Qin, "Motion planning for dual-arm space robot towards capturing target satellite and keeping the base inertially fixed," *IEEE Access*, vol. 6, pp. 26292–26306, 2018.
[4] M. Wang, J. Luo, J. Yuan, and U. Walter, "Coordinated trajectory planning of dual-arm space robot using constrained particle swarm optimization," *Acta Astronautica*, vol. 146, pp. 259–272, May 2018.
[5] Z. Vafa and S. Dubowsky, "On the dynamics of manipulators in space using the virtual manipulator approach," in *Proc. IEEE Int. Conf. Robot. Automat. (ICRA)*, Taipei, Taiwan, Mar./Apr. 2003, pp. 579–585.
[6] T. Lozano-Perez, "A simple motion-planning algorithm for general robot manipulators," *IEEE J. Robot. Autom.*, vol. 3, no. 3, pp. 224–238, Jun. 1987.

[7] J. Guan, C.-M. Lin, G.-L. Ji, L.-W. Qian, and Y.-M. Zheng, "Robust adaptive tracking control for manipulators based on a TSK fuzzy cerebellar model articulation controller," *IEEE Access*, vol. 6, pp. 1670–1679, 2017.

[8] Y. Wang, S. Jiang, B. Chen, and H. Wu, "Trajectory tracking control of underwater vehicle-manipulator system using discrete time delay estimation," *IEEE Access*, vol. 5, pp. 7435–7443, 2017.

[9] K. Tchon and J. Jakubiak, "A repeatable inverse kinematics algorithm with linear invariant subspaces for mobile manipulators," *IEEE Trans. Syst., Man, Cybern. Syst.*, vol. 35, no. 5, pp. 1051–1057, Oct. 2005.

[10] E. G. Papadopoulos, "Path planning for space manipulators exhibiting nonholonomic behavior," in *Proc. IEEE/RSJ Int. Conf. Intell. Robots Syst.*, Raleigh, NC, USA, Jul. 1992, pp. 669–675.

[11] G. Antonelli, S. Chiaverini, M. Palladino, G. P. Gerio, and G. Renga, "Cartesian space motion planning for robots. An industrial implementation," in *Proc. 4th Int. Workshop Robot Motion Control*, Puszczykowo, Poland, Jun. 2004, pp. 279–284.

[12] W. Xu, C. Li, B. Liang, Y. Liu, and Y. S. Xu, "The cartesian path planning of free-floating space robot using particle swarm optimization," *Int. J. Adv. Robotic Syst.*, vol. 5, no. 3, p. 27, Sep. 2008.

[13] Y. She, W. Xu, H. Su, B. Liang, and H. Shi, "Fault-tolerant analysis and control of SSRMS-type manipulators with single-joint failure," *Acta Astronautica*, vol. 120, pp. 270–286, Mar./Apr. 2016.

[14] S. Patel and T. Sobh, "Manipulator performance measures—A comprehensive literature survey," *J. Intell. Robotic Syst.*, vol. 77, nos. 3–4, pp. 547–570, Mar. 2015.

[15] Y. Umetani and K. Yoshida, "Workspace and manipulability analysis of space manipulator," *Trans. Soc. Instrum. Control Eng.*, vol. 26, no. 2, pp. 188–195, 2009.

[16] C. J. J. Paredis and P. K. Khosla, "Fault tolerant task execution through global trajectory planning," *Rel. Eng. Syst. Saf.*, vol. 53, no. 3, pp. 225–235, Sep. 1996.

[17] H. Dong, Z. Du, and G. S. Chirikjian, "Workspace density and inverse kinematics for planar serial revolute manipulators," *Mech. Mach. Theory*, vol. 70, pp. 508–522, Dec. 2013.

[18] H. Adbi, A. A. Maciejewski, and S. Nahavandi, "Reliability maps for probabilistic guarantees of task motion for robotic manipulators," *Adv. Robot.*, vol. 27, no. 2, pp. 81–92, Feb. 2013.

[19] Z. Vafa and S. Dubowsky, "The kinematics and dynamics of space manipulators: The virtual manipulator approach," *Int. J. Robot. Res.*, vol. 9, no. 4, pp. 3–21, Aug. 1990.

[20] G. Chen, W. Guo, Q. Jia, X. Wang, and Y. Fu, "Failure treatment strategy and fault-tolerant path planning of a space manipulator with free-swinging joint failure," *Chin. J. Aeronaut.*, vol. 31, no. 12, pp. 2290–2305, Dec. 2018.

[21] G. Chen, B. Yuan, Q. Jia, H. Sun, and W. Guo, "Failure tolerance strategy of space manipulator for large load carrying tasks," *Acta Astronautica*, vol. 148, pp. 186–204, Jul. 2018.

[22] Q. Jia, X. Wang, G. Chen, B. Yuan, and Y. Fu, "Coping strategy for multi-joint multi-type asynchronous failure of a space manipulator," *IEEE Access*, vol. 6, pp. 40337–40353, 2018.

[23] J. Tani and N. Fukumura, "Self-organizing internal representation in learning of navigation: A physical experiment by the mobile robot YAMABICO," *Neural Netw.*, vol. 10, no. 1, pp. 153–159, Jan. 1997.

[24] K. Charalampous, I. Kostavelis, A. Amanatiadis, and A. Gasteratos, "Real-time robot path planning for dynamic obstacle avoidance," *J. Cellular Automata*, vol. 9, nos. 2–3, pp. 195–208, May 2014.

[25] H. Zhang, H. Chen, and L. Wei, "Differentially constrained path planning with graduated state space," *Mechatronics*, vol. 38, pp. 132–142, Sep. 2016.

[26] X. Wenlong, S. Jianbo, and L. Zongli, "New coordination scheme for multi-robot systems based on state space models," *J. Syst. Eng. Electron.*, vol. 19, no. 4, pp. 722–734, Aug. 2008.

[27] W. L. Xie, "The research on motion planning and coordination for robot systems," Ph.D. dissertation, Shanghai Jiao Tong Univ., Shanghai, China, 2008.

[28] K. Yovchev, K. Delchev, and E. Krastev, "State space constrained iterative learning control for robotic manipulators," *Asian J. Control*, vol. 20, no. 3, pp. 1145–1150, May 2018.

[29] J. Su and W. Xie, "Motion planning and coordination for robot systems based on representation space," *IEEE Trans. Syst., Man, Cybern. Syst.*, vol. 41, no. 1, pp. 248–259, Feb. 2011.

[30] B. Wu and J. Su, "Evaluation of task realizability for robot systems in representation space," in *Proc. 10th World Congr. Intell. Control Automat.*, Jul. 2012, pp. 3816–3821.

[31] T. Suzuki and Y. Nakamura, "Planning spiral motion of nonholonomic space robots," in *Proc. IEEE Int. Conf. Robot. Automat.*, Apr. 1996, pp. 718–725.

[32] X. Chen and S. Qin, "Kinematic modeling for a class of free-floating space robots," *IEEE Access*, vol. 5, pp. 12389–12403, 2017.

[33] Y. Wang, H. Sun, G. Chen, Q. Jia, and B. Yu, "Hierarchical task planning for multiarm robot with multiconstraint," *Math. Problems Eng.*, vol. 2016, Jul. 2016, Art. no. 2508304.

[34] B. Liang and W. F. Xu, "Kinematics modeling of space robot," in *Space Robotics: Modeling, Planning and Control*, vol. 4, 1st ed. Beijing, China: Tsinghua Univ. Press, 2017, pp. 228–240, ch. 6.

[35] G. Chen, L. Zhang, Q. Jia, and H. Sun, "Singularity analysis of redundant space robot with the structure of Canadarm2," *Math. Problems Eng.*, vol. 2014, pp. 1–9, Jun. 2014.

QINGXUAN JIA (M'09) received the B.S. and M.S. degrees in mechanical engineering from the Shandong University of Technology, Shandong, China, in 1988 and 1991, respectively, and the Ph.D. degree in electromechanical engineering and automation from the Beijing University of Aeronautics and Astronautics, Beijing, China, in 2005.

He is a Professor with the School of Automation, Beijing University of Posts and Telecommunications. His research interests include space robotics, virtual reality technology, and pattern recognition.

BONAN YUAN received the B.S. degree in mechanical engineering and automation from the Beijing University of Posts and Telecommunications, Beijing, China, in 2015, where he is currently pursuing the Ph.D. degree in mechatronic engineering.

His research interests include space robotics, failure detection and recovery, and robot control method.

GANG CHEN (M'17) received the B.S. degree in mechanical design-manufacture and automation from the Beijing Institute of Petrochemical Technology, Beijing, China, in 2004, and the Ph.D. degree in mechatronic engineering from the Beijing University of Posts and Telecommunications, Beijing, in 2011.

He is an Associate Professor with the School of Automation, Beijing University of Posts and Telecommunications. His research interests include space robotics, motion planning, and control method.